Temperature Dependence of Pure CsI between 77 K and 165 K and the Performance of Wavelength Shifters

Diplomarbeit

von

Dominik Grögler

Physik Institut der Universität Zürich

Ausgeführt am CERN in der Gruppe von

Prof. Dr. C. Amsler

Betreut von

Dr. C. Regenfus und Prof. Dr. H. Pruys

Genf, im Juli 2001

Abstract

The production and spectroscopy of cold antihydrogen ($\overline{\mathrm{H}}$) is the aim of the ATHENA experiment at the European Laboratory for Particle Physics (CERN). The group from the University of Zürich is involved in the design and construction of the antihydrogen annihilation detector.

To detect the 511 keV γ's from $e^+ - e^-$ annihilation, 192 pure CsI crystals coupled to photodiodes are integrated in the ATHENA detector. The expected working temperature of the detector is around 120 K.

The purpose of this work was to measure the light yield of pure CsI as a function of temperature and to investigate ways to improve the energy resolution with wavelength shifters.

The first chapter gives a brief introduction to $\overline{\mathrm{H}}$ production and spectroscopy at ATHENA.

Fundamentals of scintillation light production and their detection by semiconductor devices to be used in the ATHENA annihilation detector are discussed in the second chapter.

In the third chapter measurements with photodiodes of the the light yield of pure CsI as a function of temperature in the range between 77 K and 165 K are presented. It could be shown, that the light yield of pure CsI measured with a photodiode had a strong dependence on temperature with a maximum at 120 K. Furthermore, the light yield could be increased by 70 % at 120 K and even 155 % at 77 K, respectively, by using fluorescent dyes as wavelength shifters.

A setup to test the completely assembled detector at low temperature in the laboratory before insertion into the experiment is presented in the fourth chapter together with first results of the detector performance.

Conclusions and important implications for the ATHENA detector can be found in the fifth chapter.

Contents

List of Figures

Chapter 1

The ATHENA Experiment

The **A**n**T**i **H**ydrog**EN** **A**pparatus[1] was designed to produce very slow antihydrogen atoms (kinetic energy below 0.1 meV) to study CPT invariance. If CPT invariance is a fundamentally conserved physical property, the masses and lifetimes of particles and their antiparticles should be the same. Also, the charges and magnetic moments should be the same but of opposite sign. If CPT invariance holds true, the fine structure, hyperfine structure and Lamb shift of antiatoms are also the same as for their matter counterparts. Therefore, the comparison of the energy levels of atoms with the energy levels of the corresponding antiatoms allows a test of CPT invariance for leptons and baryons. Since hydrogen is the simplest atom, and since its properties are known with high accuracy, antihydrogen is very suitable for testing CPT.

The transition 2s $\rightarrow$ 1s of the hydrogen atom is of special interest, because of the long lifetime of the 2s state (122 ms). The natural line width $\Delta\nu/\nu$ is therefore of the order of 5×10^{-16}, which allows a test of CPT with very high precision. This theoretically achievable accuracy is by four orders of magnitude better than current tests on CPT invariance for leptons which were done by comparing electrons with positrons.

Once the production of a sufficient amount of antihydrogen will have been accomplished, the electrically neutral $\overline{\mathrm{H}}$ atoms could be confined by a strong magnetic gradient field, which interacts with the magnetic moments of the positrons. The energy difference between the 1s and 2s levels will then be determined by 2γ recoilless spectroscopy. First the 1s state will be pumped to the metastable 2s state by Dopplerfree 2γ laser absorption (2×243 nm). Then the 2s and 2p states could

[1] ATHENA is a collaboration between CERN, Universities of Genoa and Tokyo (antiproton capture, external detectors and recombination), University of Swansea (positron accumulator), Universities of Pavia and Zürich (annihilation detector), University of Brescia (DAQ and slow control), Massachussets Institute of Technology, Universities of Aarhus and Rio de Janeiro (laser spectroscopy).

be mixed with a short electrical pulse, allowing a certain fraction of positrons to flip their spin. The $\overline{\mathrm{H}}$ atoms in the 2p state would quickly deexcite to the ground state (the 2p state of the H atom has a lifetime of $\simeq 10^{-10}$ s). The $\overline{\mathrm{H}}$ atoms in the 2s state which flipped their spin would no longer be confined (only $\overline{\mathrm{H}}$ atoms with an e^+ spin parallel to the magnetic gradient field can be confined), move to the wall of the recombination trap, and annihilate there. The energy difference between the 1s and 2s states could then be determined by a measurement of the annihilation rate of antihydrogen atoms as a function of the applied laser wavelength.

Another possible objective is a test on the weak equivalence principle (WEP). The WEP predicts, that all free falling objects feel the same gravitational acceleration, regardless of their composition. In particular, atoms and their corresponding antiatoms or particles and their corresponding antiparticles feel the same gravitational acceleration according to the WEP. The measurement of the gravitational acceleration of electrically neutral objects is easier than performing the same measurement with charged particles since they do not interact by electric forces. The WEP could be tested by ballistic measurements of the gravitational acceleration of antihydrogen in the gravitational field of the earth.

1.1 The Antiproton Decelerator

The antiprotons for the experiment are supplied by the **A**ntiproton **D**ecelerator (AD). This machine was constructed for three experiments using slow antiprotons. The ASACUSA (**A**tomic **S**pectroscopy **A**nd **C**ollisions **US**ing **A**ntiprotons) collaboration studies antiprotonic helium (a helium atom in which an electron is replaced by an antiproton) by laser spectroscopy, ATRAP (**A**ntihydrogen **TRAP**) and ATHENA both study cold antihydrogen.

Bunches of 1.5×10^{13} protons with momenta of 26 GeV/c are shot onto an iridium target to produce antiprotons. At the momentum of the maximum yield (3.5 GeV/c) they are inserted in the AD. By stochastic cooling, the momentum is reduced in two steps from 3.5 GeV/c to 2 GeV/c and then down to 0.3 GeV/c. Before the antiprotons are extracted to the experiments, the momentum is further decreased by electron cooling down to 100 MeV/c.

The AD provides ATHENA every two minutes with a 200 ns bunch of 3×10^7 antiprotons.

1.2 The Antihydrogen Apparatus

The goal of the first phase of the ATHENA experiment is the production of a sufficient amount of antihydrogen atoms ($\simeq 100 - 1000\,\mathrm{s}^{-1}$) for laser spectroscopy.

To achieve this, the following steps are necessary:

- Trapping and cooling of antiprotons and positrons.
- Recombination of antiprotons and positrons to form antihydrogen.
- Detection of antihydrogen.

The two main components of the antihydrogen apparatus are the positron accumulation trap and a superconducting solenoid which houses the positron and antiproton traps, the recombination trap and the annihilation detector (see figure 1.1). The annihilation detector can be seen in more detail in figures 1.2, 1.4, 1.5 and 1.6.

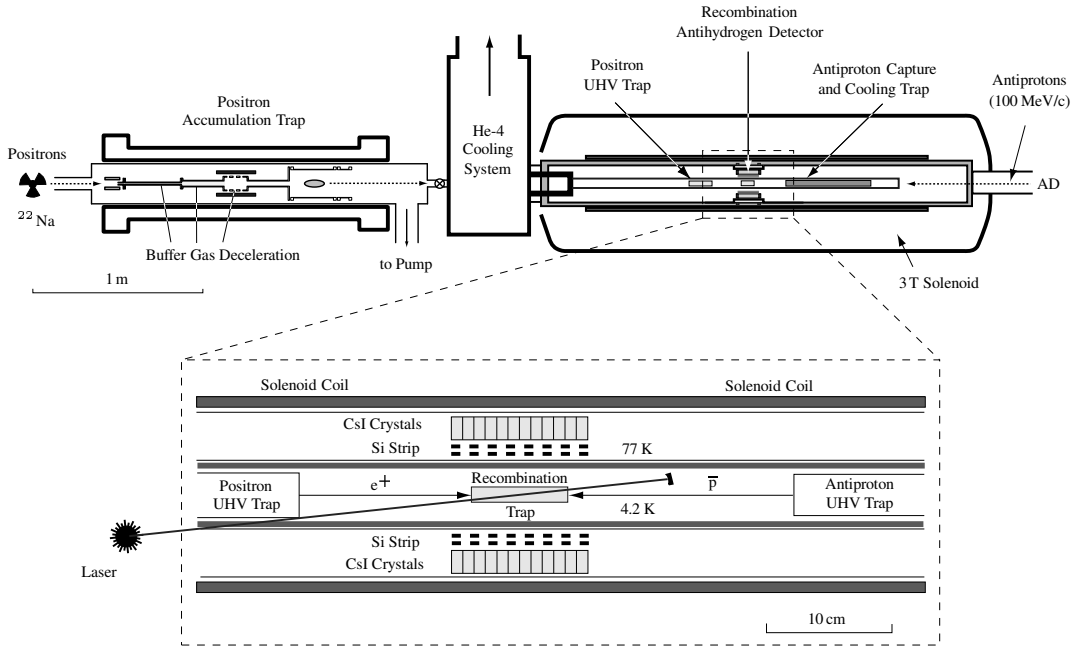

Figure 1.1: Overview of the ATHENA experiment. The inner part of the recombination region, including the annihilation detector, is shown in the enlargement at the bottom.

1.2.1 Cooling and Trapping of Antiprotons and Positrons

After the antiprotons are extracted from the AD, they pass through a silicon beam counter, which gives information on the position and size of the beam and allows

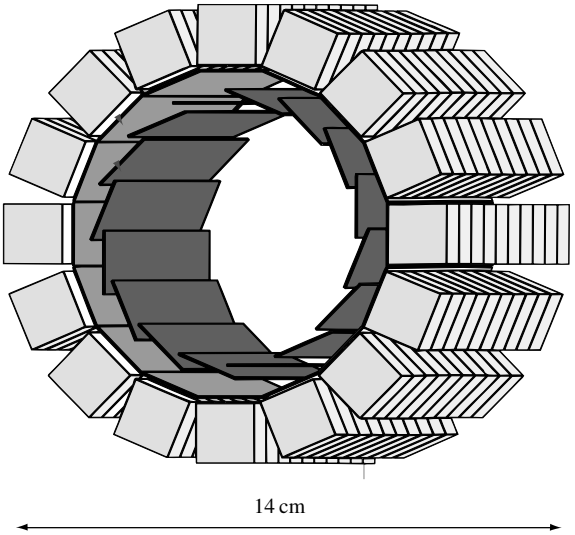

Figure 1.2: Diagram of the ATHENA detector showing the 16 rows of 12 pure CsI crystals each on the outside and the two layers of 16 double sided silicon microstrip detectors each in the inner part.

the adjustment of the beam fine steering. The beam is then degraded by an aluminum foil of $\simeq 40\,\mu$m thickness. Inside the trap, the antiprotons are reflected by a potential barrier of -15 kV. Once the antiprotons are inside the trap, an electric potential of -15 kV is applied at the entrance window. This way, the antiprotons are captured between the two potential barriers. A cold electron gas of $\simeq 3 \times 10^8$ electrons, which is inserted into the trap before injection of antiprotons, reduces the kinetic energy of the antiprotons down to a few meV. Trapping takes place in the magnetic field of the 3 T solenoid.

In recent times a good trapping efficiency could already be obtained. From a bunch of 3×10^7 antiprotons that was supplied by the AD, 16 000 antiprotons could be cooled down to kinetic energies below one eV and could then be stored for a time of more than 10 hours.

The positrons are produced by a ^{22}Na source with an activity of about 2×10^9 Bq (^{22}Na decays by electron capture or β^+ emission). The positrons are first moderated by solid neon, then by nitrogen gas and by synchrotron radiation in a magnetic field. Trapping and accumulation is very similar to the system used for the antiprotons.

At present 4×10^7 positrons can be accumulated. However, it is not yet possible to transfer the positrons to the recombination trap.

1.2.2 Recombination of Antiprotons and Positrons

The two basic principles to form $\overline{\mathrm{H}}$ are spontaneous radiative recombination and three body recombination. The simplest way to form $\overline{\mathrm{H}}$ is spontaneous radiative

recombination:

$$e^+ + \overline{p} \longrightarrow \overline{H} + h\nu$$

Another way to form $\overline{H}$ is three body recombination:

$$e^+ + e^+ + \overline{p} \longrightarrow \overline{H} + e^+$$

In both recombination processes the excess momentum and energy are carried away by the photon and the positron, respectively. The temperature dependence of these processes ($\propto T^{-1/2}$ for spontaneous radiative recombination and $\propto T^{-4.5}$ for three body recombination) show that spontaneous radiative recombination will dominate over three body recombination by more than two orders of magnitude as the temperature in the recombination trap is $\simeq 4$ K.

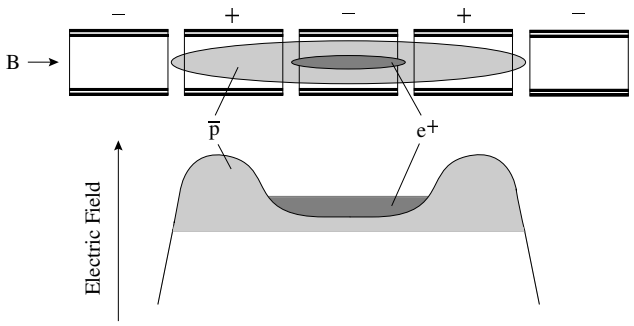

Figure 1.3: The recombination trap is a nested penning trap. Antiprotons and positrons can be held in close contact for recombination.

The accumulated antiprotons and positrons will be guided by electric fields to the recombination trap, which is a nested penning trap. This trap is built of cylindrical electrodes, which are aligned axially and are held at alternating positive and negative potentials as shown in figure 1.3. This design allows overlapping antiproton and positron plasmas for recombination.

The $\overline{H}$ yield could be enhanced by laser stimulation:

$$e^+ + \overline{p} + kh\nu \longrightarrow \overline{H} + (k+1)h\nu$$

For this the recombination trap would have to be illuminated with short pulses of a high frequency laser source. The enhancement would be in the order of one to two orders of magnitude.

1.2.3 Detection of Antihydrogen

After the electrically neutral antihydrogen atom will have been formed, confinement in the electric and magnetic field will cease and the antiatom will drift to the

trap electrodes and annihilate. When the $\overline{\mathrm{H}}$ atom will have reached the trap electrodes the positron will annihilate with an electron producing two back–to–back 511 keV γ's. The antiproton will annihilate with a nucleus and produce a number of charged and neutral pions. The neutral pions will decay instantaneously ($\tau \simeq 10^{-17}$ s) into two γ's with an energy between 50 MeV and 500 MeV. On average, three charged pions, three high energy γ's and two 511 keV γ's will be produced [1].

To prove, that the annihilation stems from antihydrogen rather than from unbound or uncorrelated antiprotons and positrons, a time coincidence between the annihilations of the antiproton and the positron has to be established. Furthermore we will require the two 511 keV γ's to be emitted back–to–back from the annihilation vertex of the antiproton.

For charged particle tracking and vertex reconstruction, the charged pions will be detected by 32 silicon microstrip detectors, which are aligned in two cylindrical layers of 16 each (see figures 1.2, 1.5 and 1.6). The front side of each strip detector is divided into 384 strips along the detector axis (z coordinate) to measure the azimuthal angle. The back side of each strip detector is divided into 64 pads aligned perpendicular to the strips to measure the z coordinate. The position resolution of the azimuthal angle has been measured to be better than 25 μm. The

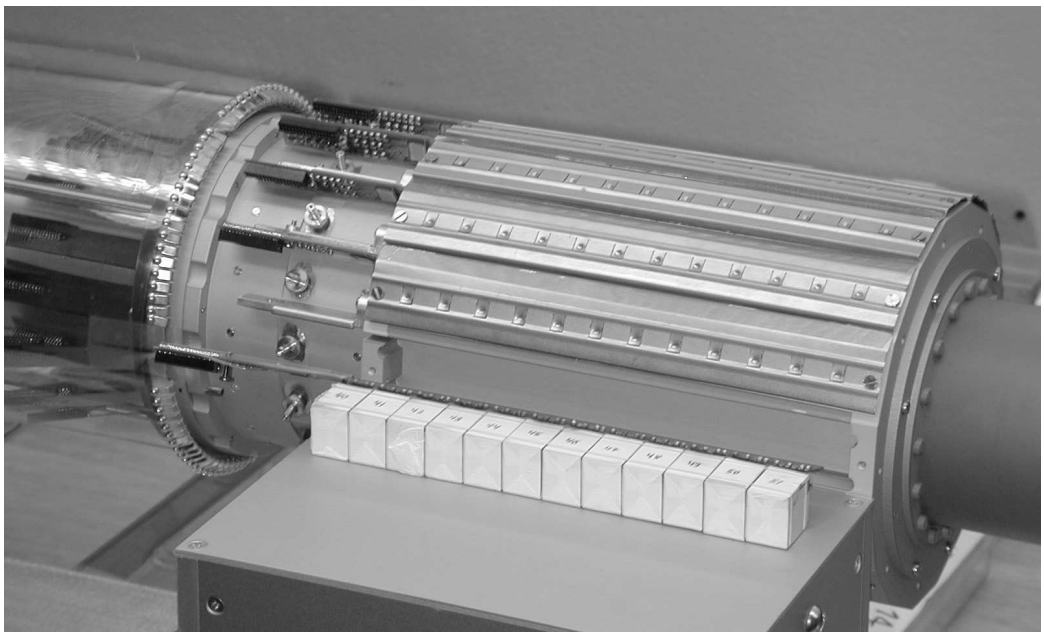

Figure 1.4: The opened ATHENA annihilation detector. One row of 12 CsI crystals wrapped into white teflon tape can be seen before installation into the detector.

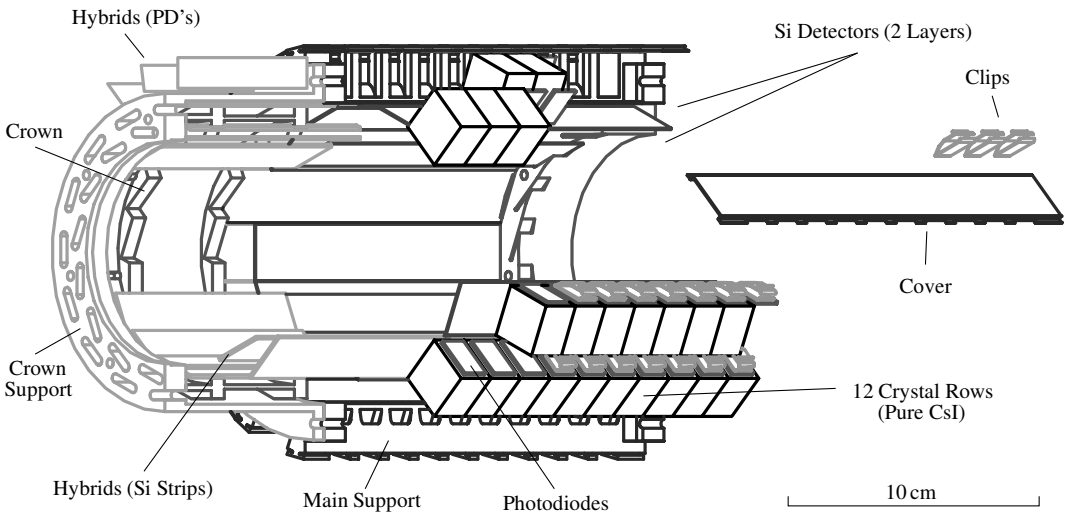

Figure 1.5: Detailed diagram of the annihilation detector.

resolution in the z direction is in the order of 300 μm.

192 scintillating pure CsI crystals are arranged in 16 rows of 12 crystals for the detection of the 511 keV back–to–back γ's (see figures 1.2, 1.4, 1.5, and 1.6). The scintillation light that will be produced by the 511 keV γ's in the crystals will be read out by silicon photodiodes. The segmentation of each row into 12 individual crystals allows a spatial resolution of $\simeq 1$ cm.

The γ's that are produced in the decay $\pi^0 \rightarrow 2\gamma$ have energies in the range between 50 MeV and 500 MeV. At these energies, γ's will cause electromagne-

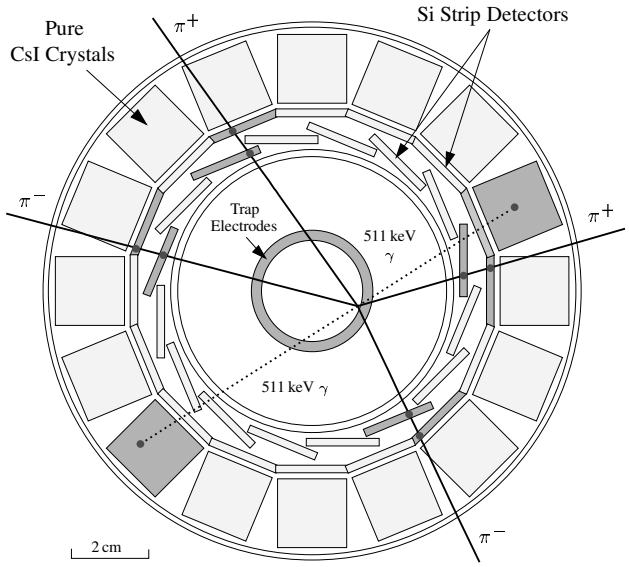

Figure 1.6: Cross section of the annihilation detector. As an example a N $\overline{\mathrm{p}} \rightarrow 2\pi^+ 2\pi^-$ annihilation is shown with the two 511 keV back–to–back γ's from $e^+ - e^-$ annihilation. The pions are detected in the silicon microstrip detectors, the γ's in the CsI crystals (Monte Carlo simulation).

tic showers in the CsI crystals and also in materials surrounding the detector. In an electromagnetic shower the primary γ creates electrons and positrons by pair production. Both electrons and positrons create secondary γ's by bremsstrahlung. The secondary γ's can then undergo the same interaction as the primary γ. This way a cascade of γ's, electrons and positrons is produced. The shower will stop when the energy loss by ionisation dominates over bremsstrahlung for the electrons and positrons and when Compton scattering dominates over pair production for the γ's. As the positrons loose their energy by bremsstrahlung and ionisation losses they will eventually annihilate and produce two 511 keV back–to–back γ's, which will contribute to the background in the CsI crystals.

Chapter 2

Detection of γ–Radiation

In this chapter the detection of γ–radiation in the energy range of 10 keV to 1 MeV will be discussed. The focus of attention will be on pure CsI scintillation crystals used for energy conversion of primary γ's and on silicon photodiodes for readout of the scintillation light. The photodiodes manufactured by SINTEF for the ATHENA annihilation detector will be of particular interest.

The most important requirements that a detector of γ–radiation has to fulfill, are:

- Conversion of the γ energy in kinetic energy of primary electrons by photoelectric absorption, Compton scattering or pair production.
- Production of secondary electron–hole pairs, electron–ion pairs or the excitation of atoms by the primary electrons.
- Collection of the secondary charge carriers or of the light that is produced by recombination of the secondary charge carriers or by deexcitation of the atoms.

For energies below 1 MeV only photoelectric absorption and Compton scattering occur, while pair production is possible at energies above 1022 keV (two times the rest mass of the electron) and only plays an important role at higher energies.

Because the detection of 511 keV γ's from $e^+ - e^-$ annihilation is of high importance for the ATHENA detector, a Monte Carlo simulation was done to estimate the detection efficiency of 511 keV γ's in pure CsI [2]. In this simulation a point like source of monoenergetic 511 keV γ's, which irradiates a cubic pure CsI crystal was assumed. Two cases were distinguished in this Monte Carlo simulation:

1. The γ's give all their energy directly to an electron by photoelectric absorption.

2. The γ's are first Compton scattered, then they either give the rest of their energy to an electron by photoelectric absorption or they are again Compton scattered.

Further interactions of the remaining Compton scattered γ's were not taken into account.

A simulation with 10 000 primary 511 keV γ's has shown that 57 % (5721 events) undergo an interaction in the crystal. Of these, 21 % (1194 events) by photoelectric absorption and 79 % (4527 events) by Compton effect. Of the Compton scattered γ's 56 % (2553 events) undergo a secondary interaction. 46 % (1174 events) by photoelectric absorption and 54 % (1379 events) by Compton scattering. The contribution of γ's to the full energy peak which loose all their energy directly by photoeffect is about one half. The other half comes from γ's which undergo a Compton scattering followed by photoelectric absorption. In this model, the probability, that a 511 keV γ contributes to the full energy peak, is about 24 % (2368 events).

The CsI calorimeter of the ATHENA detector covers a solid angle of approximately 66 % of 4π. This yields a detection efficiency of about 16 % for a single 511 keV γ and about 3.8 % for the detection of two 511 keV back–to–back γ's.

2.1 Production of Scintillation Light

An ideal scintillator has a high light output for good energy resolution and fast time characteristics to be able to deal with high particle fluxes.

Inorganic scintillators are known to have the highest light yield. One of the most common inorganic scintillators, Caesium iodide activated with thallium (CsI(Tl)), has almost 400 % total light output compared to one of the best organic scintillator (Anthracene) [3].

However, most inorganics have a very slow response which can be in the order of μs, whereas the response for organics and plastics is from a few ns to several tenths of ns.

The process of scintillation in inorganics involves energy transfer of the incoming particle to valence electrons which are lifted in the conduction band. The so created electron–hole pairs can then travel free in the crystal and emit scintillation light by recombination.

In many materials the energy needed to create one electron–hole pair is roughly the same energy that is released when the pair recombines. In this case all produced light is reabsorbed. To overcome this problem, many inorganic scintillators are impurified by certain substances (activators). For this, a small amount of another substance is added to the pure scintillatior. By doing this, the bandgap

between the valence band and the conduction band in the pure crystal is modified around the activator atoms. The activator has to be chosen in such a way that it creates possible energy states in the bandgap of the pure scintillator which can be occupied by electrons. A created hole will then move to an activator atom and ionize it, since the energy needed to ionize an activator atom is lower than for ionizing the pure scintillation material. The electron is free to move in the crystal and will preferably recombine at the ionized activator atoms by releasing a photon. Because this photon is not energetic enough to create another electron–hole pair, it will contribute to the total light yield. CsI(Tl) is often chosen because of its high efficiency.

For a detailed discussion of the scintillation mechanisms in activated inorganics and other materials see [3].

2.1.1 Scintillation in Pure CsI

Compared to the number of activated inorganics that is known to have scintillating properties only a few inorganics are known to scintillate in their pure state. Also the scintillation mechanisms in pure inorganics are much less understood. With regard to the electromagnetic calorimeter of the ATHENA detector which is made of pure CsI crystals with photodiode readout, some characteristic scintillation properties of pure CsI will be outlined.

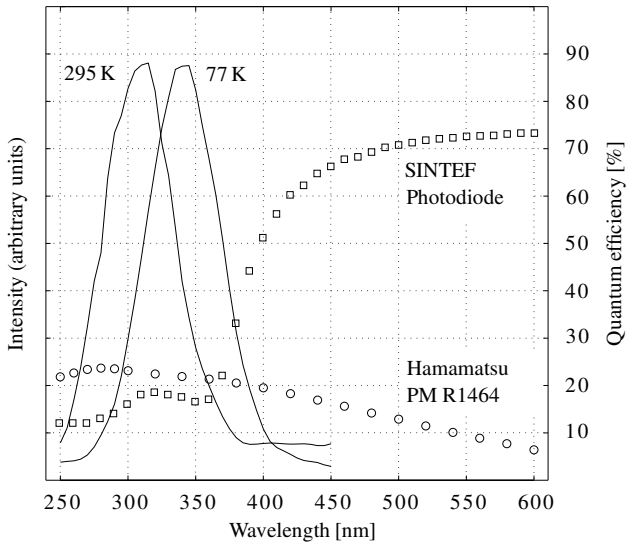

Figure 2.1: Emission spectrum of pure CsI at two different temperatures (taken from [4]) and quantum efficiencies of a Hamamatsu photomultiplier R1464 and a SINTEF photodiode.

At room temperature, pure CsI has only about 6 % of the light output of CsI(Tl) [4, 5]. However, the fast component which has its maximum emission at a wavelength of 305 nm has a decay time of only 2 – 20 ns. Most inorganics have decay times of hundreds of ns up to several μs, with the exception of BaF_2 which has a

decay time in the order of 1 ns (fast component). At low temperature the properties of pure CsI change drastically. At 77 K the decay time of the slow component decreases by almost two orders of magnitude [3, 5]. Because of the low particle flux, fast respond is not of primary concern for ATHENA. On the other hand, a high light yield is of vital importance to achieve a good energy resolution. Measurements of the light yield of pure CsI as a function of temperature using photodiodes will be presented in chapter 3 along with methods to improve on the efficiency by the use of wavelength shifters.

2.2 Silicon Photodiodes

The technology of the production of regular silicon crystals with low impurities and the techniques to dope them in a well defined manner are highly advanced. Silicon has a bandgap of about 1.1 eV and on average 3.6 eV are necessary for the creation of one electron–hole pair. This quantity is almost independent of the energy and type of particle that passes the detector. In comparison to photomultipliers, photodiodes are very small, have a high quantum efficiency, a low power consumption and they are almost insensitive to magnetic fields. All of these qualities are essential for the ATHENA detector.

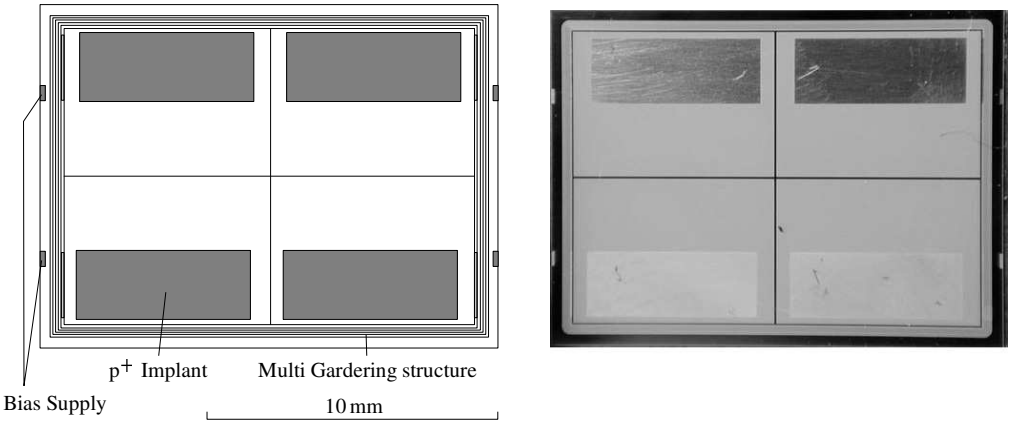

Figure 2.2: The SINTEF photodiode used for ATHENA. In the picture, the lower two of the four aluminum coated pads are oxidized, whereas the oxide was scratched off from the upper two pads.

The SINTEF photodiodes for the ATHENA detector consist of n^- doped silicon with four separate p^+ implants which are coated with aluminum for the electrical contacts (see figure 2.2). If all p^+ implants are readout separately, the diode works as if four independent diodes were used. The reason for this design is the fact that the noise of the preamplifier as a function of the input capacitance

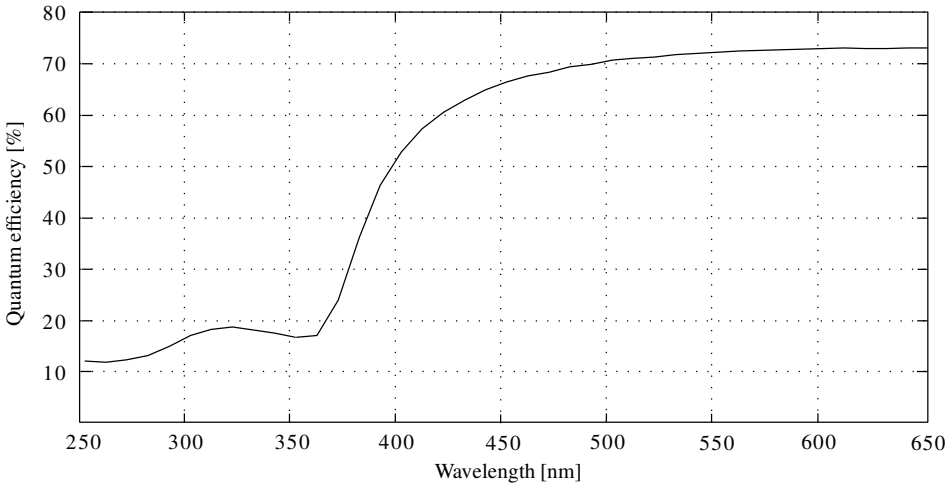

Figure 2.3: Measured quantum efficiency of the photodiodes as a function of wavelength in the range of 250 nm to 650 nm. The errors are in the order of 1 %.

is proportional to the square root of the capacitance. Therefore, operating four diodes separately leads to a signal/noise ratio that is twice as high compared to operating four diodes in parallel (it turned out, however, that this theoretically achievable figure could not be reached). On the other hand, triggering of the signals is much simpler when all pads are connected and it could be shown that an energy resolution of better than 12 % can still be reached (see figure 3.6) which is sufficient to separate the 511 keV γ's from noise. For those reasons the four pads are connected to each other in the current design.

A thin SiO_2 layer was applied onto the entrance window of the photodiode to optimize its quantum efficiency for UV light at 340 nm, where the emission spectrum of pure CsI has its maximum at a temperature of 77 K (see figure 2.1). The thickness of the layer was chosen for UV light to undergo constructive interference at the crossing of the SiO_2 layer to the n^+ layer. Unfortunately, this attempt was not successful. The quantum efficiency in the range between 250 nm and 350 nm is below 20 % (see figure 2.3). The maximum at 320 nm is probably due to oscillations of constructive interference in the SiO_2 layer.

The entrance window is on the n–side of the diode. Because depletion spreads out beginning at the p–side, the diode has to be fully depleted to convert all incoming light into electron–hole pairs. Full depletion can be reached at a bias voltage of $\simeq 30$ V.

To position the diode as directly as possible to the CsI crystal the surface of the entrance side has to be as flat as possible. Therefore not only the signal readout but also the bias supply is on the backside of the diode (see figure 2.2). There are four bias connections which are coupled to a bias ring on the front side of the

Figure 2.4: Setup for measuring the quantum efficiency of the photodiodes.

diode. A problem that arises from this design are surface currents between the pads and the bias connections on the the backside of the diode. This can lead to high leakage currents. To reduce those surface currents, a multi gardering structure which can be held at ground level, was applied between the the aluminum covered p^+ implants and the edges of the photodiode.

The quantum efficiency of the photodiode as a function of wavelength was measured with the apparatus shown in figure 2.4. A light beam of defined wavelength was sent to a mirror where it was split into two separate beams. A reference cell was then illuminated by one of these beams, the SINTEF photodiode with the other one. The currents were then measured both in the reference cell and in the SINTEF diode. Before comparing the two, their respective dark currents were substracted. The reference cell was made out of three photodiodes, positioned in such a way, that incoming light which was reflected at the surface of one photodiode reached one of the other photodiodes. This ensured, that almost all incoming light was converted into electron–hole pairs and in good approximation the quantum efficiency of the reference cell could be taken as 100 %. Therefore, normalizing the data of the photodiode to the data taken with the reference cell directly yielded its quantum efficiency.

A piece of capton with electrical lines mounted on them was designed to provide for the electrical contacts of bias and signal lines. It was planned to glue it on the back side of the diode and then to bond from these lines to the pads and bias connections. This procedure resulted in very high ohmic contacs. It turned out that the aluminum layer on the pads oxidizes very fast and therefore bonding was

not successful to establish good contacs. This can be seen in figure 2.2 where the lower two pads are oxidized, whereas the oxide was scratched off from the upper two pads. To avoid this problem, now thin cables are glued onto the backside and the side of the diode with a temperature resistant two component glue and then contacted with a conductive silver paint after scratching away the oxide layer with a toothpick. Another advantage is the fact, that the glued cables are mechanically much more robust than the bonded lines.

Chapter 3

Light Yield of Pure CsI between 77 K and 165 K

As explained in chapter one, in the ATHENA experiment annihilating antihydrogen will produce a number of charged and neutral pions (from $\overline{\mathrm{p}}$–nucleus annihilation) and two back–to–back γ's, each with an energy of 511 keV (from $\mathrm{e}^+ - \mathrm{e}^-$ annihilation). These γ's will be detected by the measurement of scintillation light in pure CsI crystals. To achieve this, the scintillation light is collected and directed onto a photodiode, where the produced free charge carriers can be collected and measured.

The objective of the measurements described in this chapter was to determine the number of electron–hole pairs/MeV produced in the photodiode as a function of temperature in the range between 77 K and 170 K.

First measurements were performed with a CsI crystal wrapped in white teflon tape, followed by measurements using a wavelength shifter for the scintillation light. Furthermore, the influence of coupling the diode to the crystal with or without silicon grease and differences between individual diodes were investigated.

In order to be able to optimize the ATHENA detector, all tests were made using the same type of diodes and pure CsI crystals which are being used in the completed detector.

3.1 The Setup

The photodiodes (especially made for ATHENA by SINTEF, Norway) and the pure CsI crystals (cuboids with dimensions of $13.0 \times 17.1 \times 17.6\,\mathrm{mm}^3$, obtained from CRISMATEC) were wrapped into diffuse reflecting teflon tape to collect as much scintillation light as possible. For the measurements at low temperature, the crystal and diode were mounted inside a vacuum tight stainless steel box which

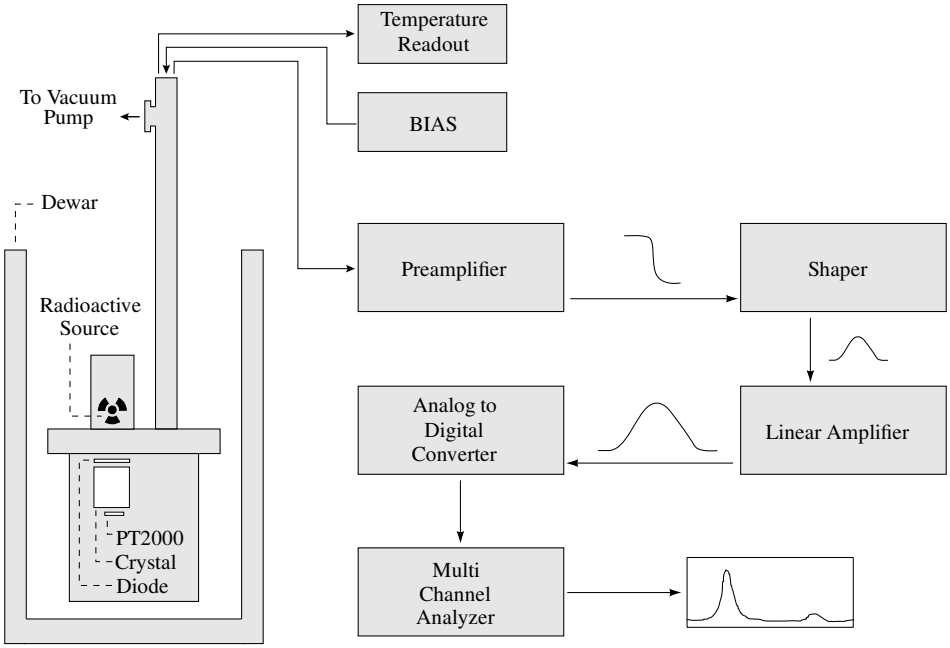

Figure 3.1: γ–rays from a radioactive source produce light in a scintillating crystal. This light illuminates a photodiode. The collected free charge carriers are read out by a charge sensitive preamplifier which creates a pulse. This pulse is processed by a shaper and further amplified by a linear amplifier. The pulse is then digitized by an analog to digital converter (ADC) for counting the pulses with the multi channel analyzer. Temperature is read out by a PT2000 temperature sensor.

could be lowered into a dewar filled with liquid nitrogen. On top of the box a pipe was installed to house the lines for signal readout and bias supply, the vacuum pump connection and a line for temperature readout with a PT2000 sensor. Cooling the system was done with liquid nitrogen, warming up with a hair–dryer.

Annihilation γ's with energies higher than 500 keV pass through the photodiode with negligible interaction, depositing all their energy in the CsI crystal, whereas the lower energy γ's of 22 keV and 88 keV used for calibration, deposit all their energy directly in the photodiode. A diagram of the setup can be seen in figure 3.1, a photograph of the opened box with a mounted crystal in figure 3.2.

3.1.1 Amplification, Signal Shaping and Processing

For preamplification of the signal that came from the photodiode, a Canberra 2003 BT charge sensitive preamplifier was used. It was located outside the cryostat. To achieve the maximum signal/noise ratio, this signal was then processed

Figure 3.2: Housing of the CsI crystal (wrapped in white teflon tape) and the photodiode used for the test. The larger pipe was used to insert radioactive sources, the smaller ($\simeq$ 0.7 m long) housed lines for temperature and signal readout and for the bias supply. Also seen is the connection of the PT2000 temperature sensor on top of the crystal.

by a Tennelec TC 205 A amplifier with 8 μs shaping time (semi gaussian shaper). To adjust the pulse to a maximum voltage of 8 V an Ortec Multi linear amplifier was used. 8 V was the voltage limit for the ADC (FAST 7070). By comparing pulse height spectra taken at different threshold levels, the best setting to exclude noise from the spectra was chosen for the ADC. The multichannel analyzer system (Compe MCD/PC) had 512 channels and processed the pulse height spectra with a PC. The system worked highly linear. This was previously shown by taking pulse height spectra of test pulses created in a pulse generator.

The shaping time had to be selected carefully since it can strongly influence the pulse height spectrum to be measured and even lead to meaningless measurements. The two main features that are affected by the shaping time are peak pile–up and noise.

Peak pile–up occurs when two pulses are so close together that the processing unit is not able to distinguish them. This is the case, when the shaping time is set too high or when the counting rates are too high, respectively. The result is a distorted pulse which can lead to significant changes in the differential pulse height spectrum, including the appearance of lines which have no physics meaning. The probability P of two pulses being separated by at least the shaping time τ is given

by Poisson statistics:

$$\mathrm{P}(t > \tau) = e^{-n\tau} \tag{3.1}$$

where n is the true event rate in the detector. Therefore, to reduce peak pile–up, it is desirable to choose a short shaping time. The used ^{109}Cd source caused counting rates of $\simeq 50\,\mathrm{s}^{-1}$ in the detector, the ^{22}Na source rates of $300-600\,\mathrm{s}^{-1}$. For these low rates equation (3.1) leads to P$= 99.96\,\%$ for ^{109}Cd and P$= 99.52\,\%$ for ^{22}Na with a shaping time τ of $8\,\mu$s (this is longest shaping time to which the Tennelec TC 205 A can be set). Therefore peak pile–up is negligible.

Regarding the shaping time, only two kinds of noise are of importance: Serial noise (thermal noise) and parallel noise (leakage current). The dependence of serial noise $\mathrm{N_S}$ from the shaping time τ is:

$$\mathrm{N_S} \propto \frac{1}{\sqrt{\tau}} \tag{3.2}$$

For parallel noise $\mathrm{N_P}$ holds true:

$$\mathrm{N_P} \propto \sqrt{\tau} \tag{3.3}$$

The total noise adds up quadratically. It falls with increasing shaping time due to serial noise, undergoes a minimum and then increases due to parallel noise. The best signal/noise ratio was determined experimentally by comparison of pulse height spectra taken with different shaping times. The best energy resolution was achieved with a shaping time of $8\,\mu$s.

Detailed discussions on shaping time effects and noise sources can be found in refs. [3, 6, 7].

3.2 Measurements

The objective of the measurements was to determine the number of electron–hole pairs/MeV produced in the photodiode as a function of temperature in the range between 77 K and 165 K.

A ^{22}Na source was used for these measurements. ^{22}Na decays by β^+ emission or electron capture (EC) to the first excited state of ^{22}Ne. The positrons annihilate with electrons and produce two 511 keV back–to–back γ's in the source itself. The excited state of ^{22}Ne decays by emission of a 1275 keV γ–ray to the ground state. A pure CsI crystal was irradiated by these 511 keV and 1275 keV γ's. The scintillation light that was then produced in the crystal, reached the photodiode – directly or after reflection on the teflon tape, in which the crystal was wrapped – and the pulse height distribution was measured with the setup presented in figure

3.1. The positions of the 511 keV and the 1275 keV peaks are a direct measure of the number of electron–hole pairs produced in the photodiode.

The photodiode was coupled to the crystal with the Pâte 7 silicon grease from RHODORSIL SILICONES, France. This grease was chosen because it stays viscous at low temperature, whereas others get hard and brake apart at low temperature. Two layers of diffuse reflecting white teflon foil were wrapped around each side of the crystal to collect as much scintillation light as possible and also to hold the diode firmly in the correct position. The crystal was fixed inside the box with a clamp as shown in figure 3.2. To make the box vacuum tight an indium seal was used. The vacuum pump was able to reach a vacuum of 0.02 – 0.04 mbar.

Both diodes and crystals were thoroughly cleaned with aceton before each measurement to remove dirt and grease residuum. For a good contact between the photodiode and the crystal it was vital for the surface of the crystal to be absolutely flat. This was ensured by polishing the crystal. Approximately 1 mm^3 of silicon grease was then applied onto the surface of the crystal. Excess grease was squeezed out by pressing the diode against the crystal (see 3.2.6 for tests without grease).

To stress the diode as little as possible, cooling down from room temperature to 77 K was performed by lowering the box into the dewar just above the level of liquid nitrogen. By avoiding direct contact of the box with liquid nitrogen, cooling down was very gentle and took about two hours. As soon as the temperature stabilized at 77 K, the measurements were performed. To shorten the time needed for warming up, hot air was blown into the dewar with a hair–dryer, raising the temperature by about 5 K for each point to measure. It was possible to warm up in such a way that temperature stayed stable for a few minutes at each measuring point (only one minute was needed to take one pulse height spectrum). The covered temperature range was from 77 K to 165 K. The limit at 165 K was predetermined by the used setup. For temperatures above 165 K the signal was so low that it could not to be separated from noise anymore.

3.2.1 Energy Calibration

In order to get the number of electron–hole pairs from the measured peak positions, an absolute energy calibration was needed. A ^{109}Cd source was used for this. ^{109}Cd decays by electron capture to an excited state of ^{109}Ag which deexcites to the ground state by emission of a 88 keV X–ray. Recombination of the ^{109}Ag atom then results in the emission of a 22 keV Ag K x–ray. At these energies, the incident γ's are absorbed completely in the photodiode. The photodiode was positioned between the source and the crystal (see figure 3.1). Since the relative distance of the two peaks is known (the linearity of the electronic chain was confirmed previously) and a 88 keV γ has four times as much energy as a 22 keV

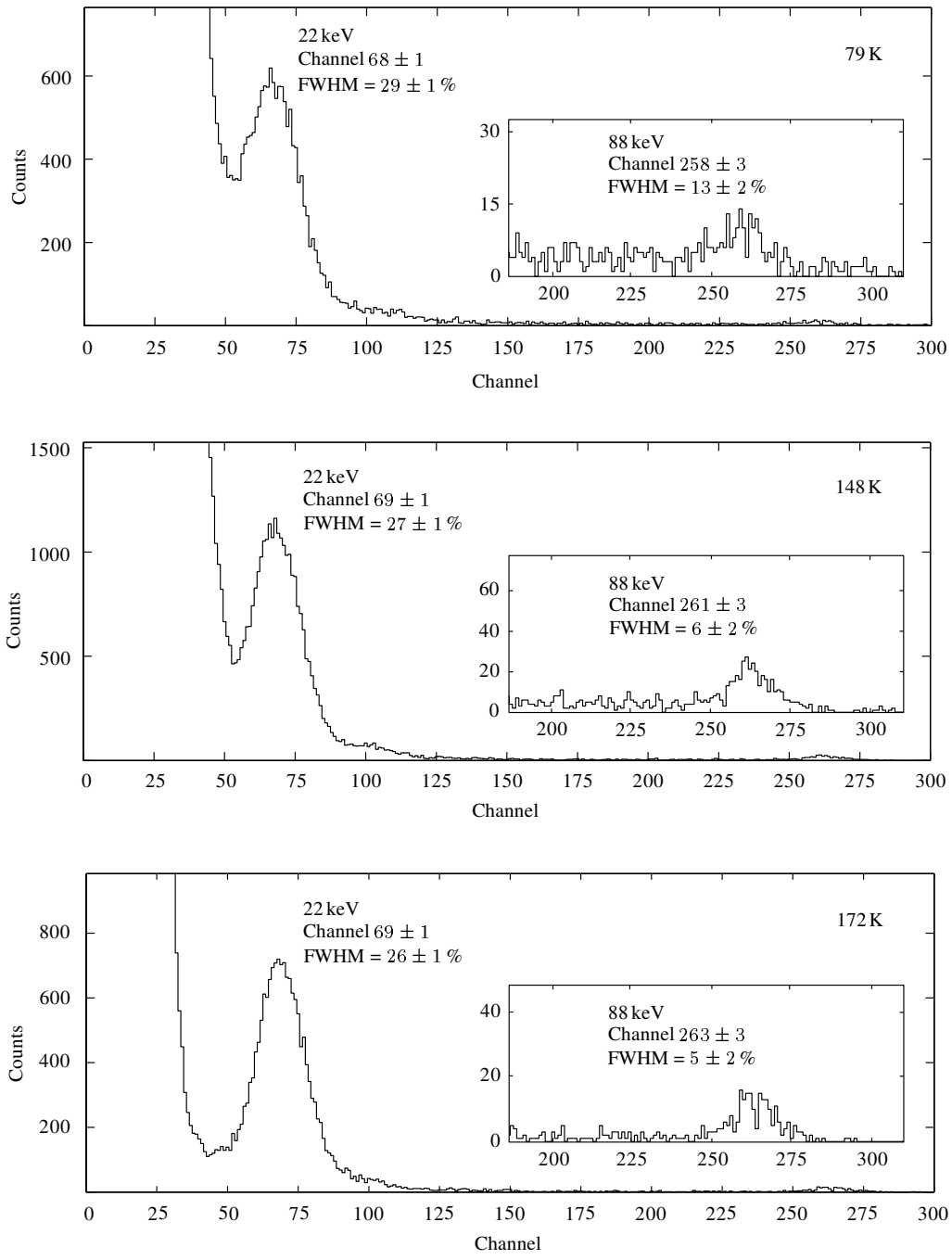

Figure 3.3: Calibration spectra taken with a ^{109}Cd source at three different temperatures with the fit parameters of the peaks. The two peaks are produced by energy deposit of the 22 keV and 88 keV X–rays directly in the photodiode.

γ, the following is true:

$$4 \cdot (\mathrm{ch}_{22} - \mathrm{ch}_0) = \mathrm{ch}_{88} - \mathrm{ch}_0 \tag{3.4}$$

where ch_{22} and ch_{88} are the positions of the 22 keV peak and the 88 keV peak, respectively and ch_0 is the corresponding channel to 0 keV. ch_0 is then given by:

$$\mathrm{ch}_0 = \frac{4 \cdot \mathrm{ch}_{22} - \mathrm{ch}_{88}}{3} \tag{3.5}$$

The calibration spectra seen in figure 3.3 lead to $\mathrm{ch}_0 = 4.7 \pm 1.7$.

On average, the energy required to produce one electron–hole pair in Si is 3.6 eV [8]. Therefore 6100 electron–hole pairs can be produced by a 22 keV γ and 24400 electron–hole pairs by a 88 keV γ, which leads to the calibration factor f:

$$f = \frac{6100}{\mathrm{ch}_{22} - \mathrm{ch}_0}\,\text{electron–hole pairs/channel} \tag{3.6}$$

Using the 88 keV peak, f can also be derived by:

$$f = \frac{24400}{\mathrm{ch}_{88} - \mathrm{ch}_0}\,\text{electron–hole pairs/channel} \tag{3.7}$$

Over a period of five months, calibration changed by no more than three channels. Furthermore, the peak positions are found to be independent of temperature. They change by only one channel for the 22 keV peak and by five channels for the 88 keV peak respectively, which is within the error limits (see figure 3.3).

3.2.2 Light Yield of Pure CsI

As explained in section 3.2, the light yield of pure CsI was measured by irradiating the crystal with γ–rays that had energies of 511 keV and 1275 keV and were emitted by ^{22}Na source. Taking the calibration into account, the number of electron–hole pairs/MeV produced in the photodiode could then be determined by the peak positions of the 511 keV and 1275 keV γ's.

Using f from equation (3.6) and the 511 keV peak position ch_{511}, the number of electron–hole pairs/MeV N_{511} is given by:

$$\mathrm{N}_{511} = f\left(\frac{\mathrm{ch}_{511} - \mathrm{ch}_0}{0.511}\right) \tag{3.8}$$

Similarly, the number of produced electron–hole pairs/MeV N_{1275} is given by the measured 1275 keV peak position ch_{1275}:

$$\mathrm{N}_{1275} = f\left(\frac{\mathrm{ch}_{1275} - \mathrm{ch}_0}{1.275}\right) \tag{3.9}$$

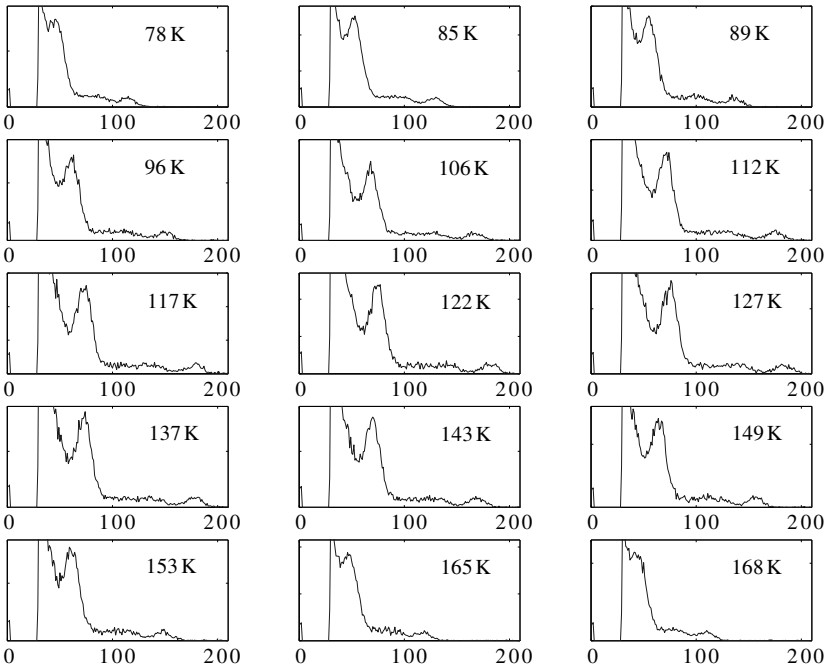

Figure 3.4: ^{22}Na pulse height spectra in the range between 78 K and 168 K taken with a pure CsI crystal and photodiode readout. Pulse height (in arbitrary units) is plotted against channel number.

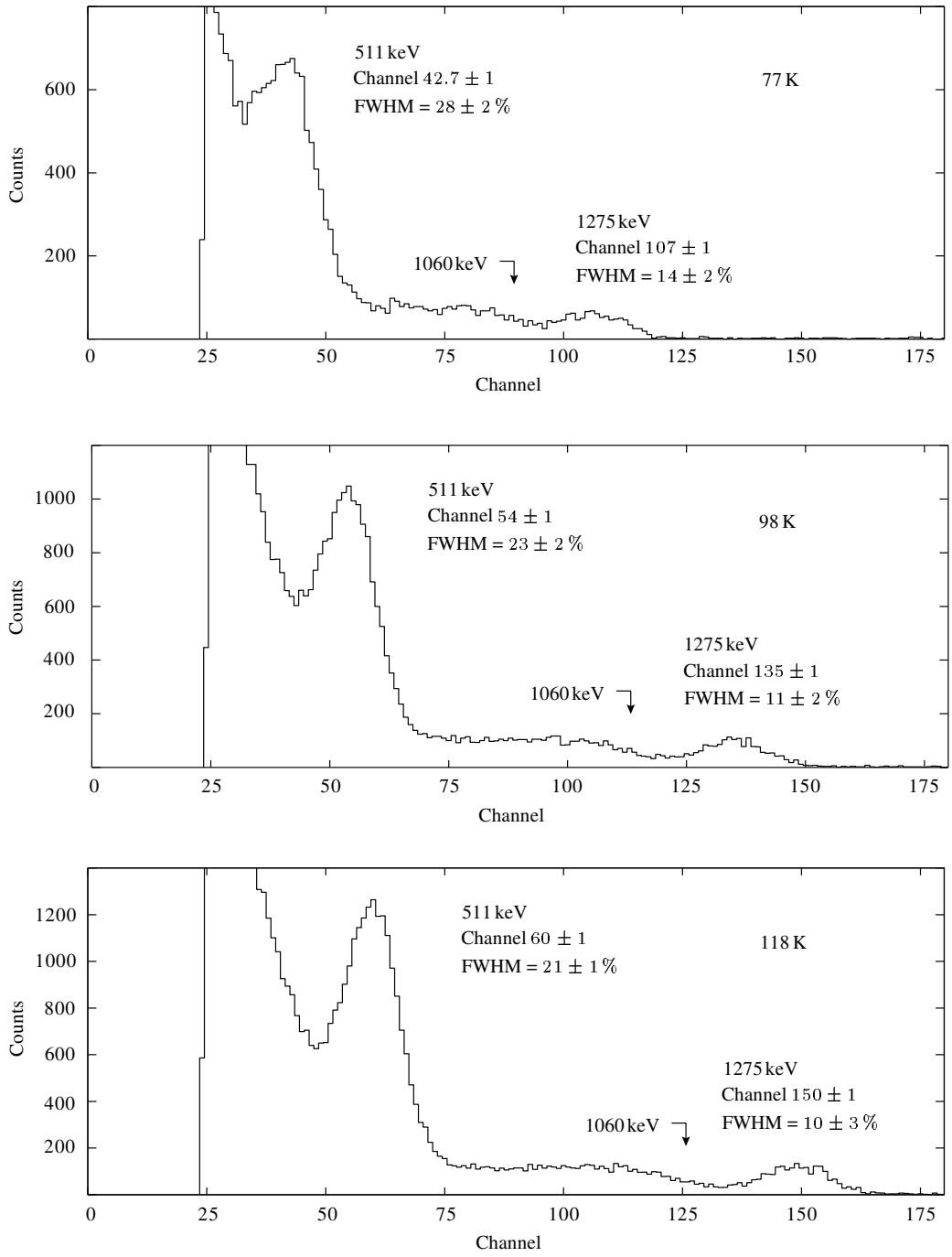

Figure 3.5: ^{22}Na pulse height spectra at three different temperatures taken with a pure CsI crystal and photodiode readout. Peak positions were fitted.

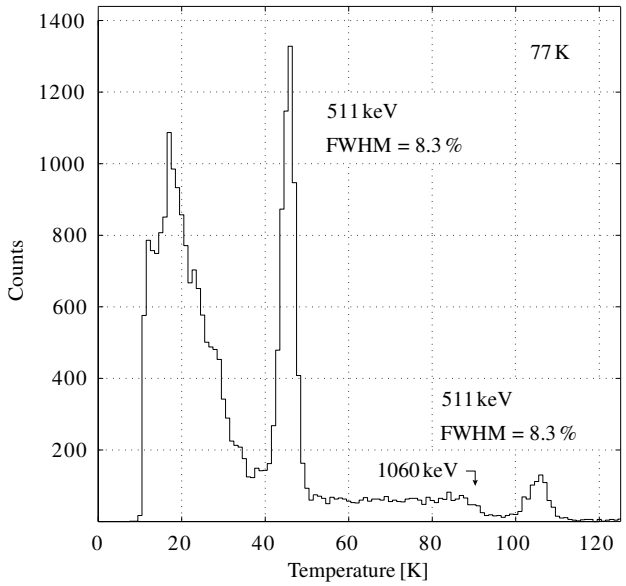

Figure 3.6: ^{22}Na pulse height spectrum taken with a pure CsI crystal and photodiode readout at a temperature of 77 K. The electronics of the final ATHENA setup were used.

Since the electronic system was linear in this energy range, N_{511} is equal to N_{1275}. For each temperature to be measured, a pulse height spectrum was taken. From these pulse height spectra the number of produced electron–hole pairs/MeV could be derived. In figure 3.4 pulse height spectra taken at 15 different temperatures in the range between 78 K and 168 K are shown. It can be seen that the peak position increases with increasing temperature up to 120 K and then falls again with further increasing temperature. In figure 3.5 three pulse height spectra can be seen in more detail. The low resolution (FWHM = 20 – 30 % for the 511 keV peak and 10 – 14 % for the 1275 keV peak) is mainly due to the long cables from the photodiode to the preamplifier ($\simeq 0.8$m) which introduce much noise to the system. Using the final ATHENA setup, noise can be reduced, as can be seen in figure 3.6, resulting in FWHM = 8.3 % for the 511 keV peak and 8.3 % for the 1275 keV peak respectively.

The position of the Compton edge for a pulse height spectrum of mono energetic γ–rays with an energy E_γ is given by:

$$E_C = E_\gamma \left(\frac{2 \cdot \frac{E_\gamma}{m_0 c^2}}{1 + 2 \cdot \frac{E_\gamma}{m_0 c^2}} \right) \tag{3.10}$$

where $m_0 c^2$ is the rest energy of the electron. For an energy of 1275 keV the Compton edge is at $E_C = 1060$ keV, explaining the plateaus in the pulse height spectra shown in figures 3.5 and 3.6.

The number of produced electron–hole pairs/MeV as a function of temperature is shown in figure 3.7. Beginning with $9\,000 \pm 600$ electron–hole pairs/MeV at 78 K, this number rises with increasing temperature to a maximum of $12\,500 \pm 600$ electron–hole pairs/MeV at 120 K, then it falls again to $7\,000 \pm 600$ electron–hole pairs/MeV at 165 K.

As temperature falls, the total light output of pure CsI rises [9] and the maximum of the emission spectrum shifts towards longer wavelengths (see figure 2.1 and ref. [4]). This explains the behavior between 120 K and 165 K since the quantum efficiency of the SINTEF photodiodes is higher at longer wavelengths (see figure 2.3).

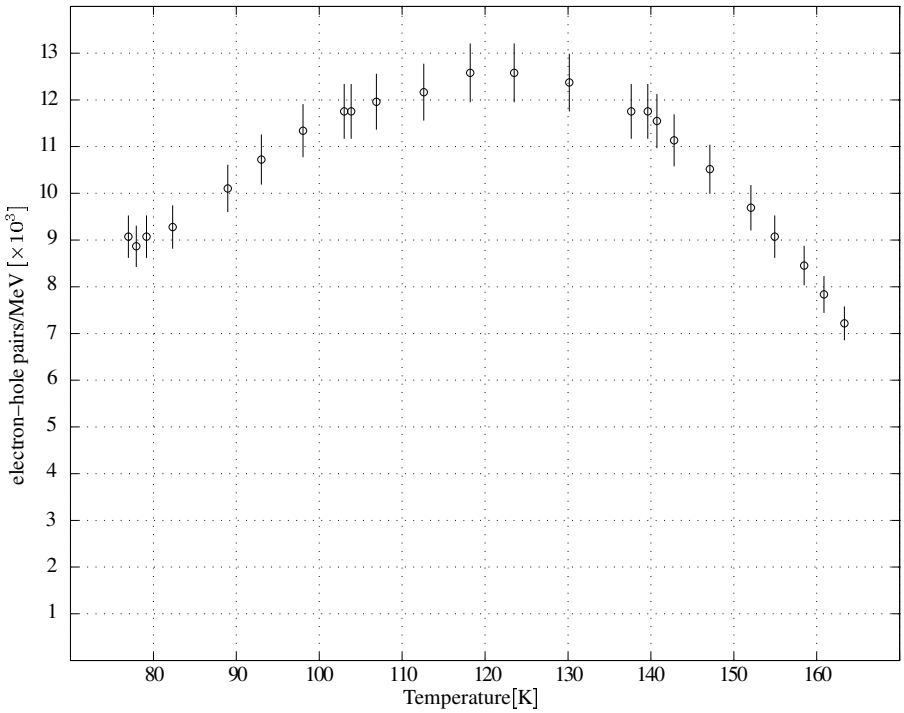

Figure 3.7: Number of electron–hole pairs/MeV as a function of temperature in the range between 77 K and 165 K. A pure CsI crystal with photodiode readout was used for this measurement.

The reason for the 28 % drop in efficiency, when decreasing temperature from 120 K down to 77 K, is not clear. Possibly it is due to variations of the maximum of the emission spectrum, which is only known for temperatures of 77 K and for room temperature [4]. Perhaps, measurements of the emission spectrum of pure CsI as a function of temperature, covering the range between 77 K and room temperature, could explain this behavior. It is also advisable to measure the quantum efficiency of the photodiodes as a function of wavelength at different temperatu-

res down to 77 K, since it is not clear if it stays constant (the quantum efficiency shown in figure 2.3 was measured at room temperature).

This measurement was repeated with five other pure CsI crystals. As well as the first one, these crystals were obtained from CRISMATEC and they all had the same dimensions. No significant changes in the observed number of electron–hole pairs/MeV could be observed. Moreover, all measurements (including the ones presented in the following sections) could be reproduced after more than 25 cooling cycles and after a time of 7 months with a deviation less than 5 %.

3.2.3 The Performance of Wavelength Shifters

The maximum of the emission spectrum of pure CsI shifts towards longer wavelengths at lower temperatures [4]. At room temperature the maximum of the spectrum is at 315 nm and increases to 345 nm at 77 K. The quantum efficiency of the SINTEF photodiodes is below 20 % for these wavelengths, but rises from 20 % to 65 % between 370 nm and 450 nm and exceeds 70 % for wavelengths of 500 nm and higher (see figure 2.3).

Therefore the use of wavelength shifters was investigated to increase the number of electron–hole pairs produced in the photodiode. The crystal was painted with a fluorescent dye which absorbs the blue UV light and reemits it at longer wavelengths. The dyes were applied by spraying them onto the crystal. The investigated dyes were: Model Master Fluorescent Red <FS28915>, made by Italeri, Italy; Sparvar Fluorescent Spray Paint Tango S.312, made by Domit AG, Switzerland; Keen Fluory, made in Italy.

The dyes were applied to all sides of the crystal, except for the side facing the diode. Qualitatively, all dyes change their efficiency as a function of temperature in the same way. The maximum at 120 K disappears, instead efficiency is constant between 77 K and 100 K, then falling with increasing temperature. Even more important, the overall performance is much better with wavelength shifters (compare figures 3.5 and 3.8). The dyes show rises up to 155 % (Sparvar), 130 % (Model Master) and 70 % (Keen) at 77 K. At 120 K the increases are still 70 % (Sparvar), 50 % (Model Master) and 18 % (Keen). This leads to a maximum number of created electron–hole pairs/MeV of $23\,000 \pm 600$ (Sparvar), $21\,000 \pm 600$ (Model Master) and 15500 ± 600 (Keen) as can be seen in figure 3.9.

The Sparvar spray paint started to flake off the crystal very quickly. After two cooling cycles at most the crystal had to be repainted, whereas the Model Master and Keen dyes stayed on the crystal undamaged for at least two cooling cycles, sometimes for more than five cooling cycles.

Covering the crystal with either one, two or three layers of dye did not lead to significant changes in light yield. Even a very thin layer of dye is sufficient for wavelength shifting (light shining through the crystal when held against sunlight).

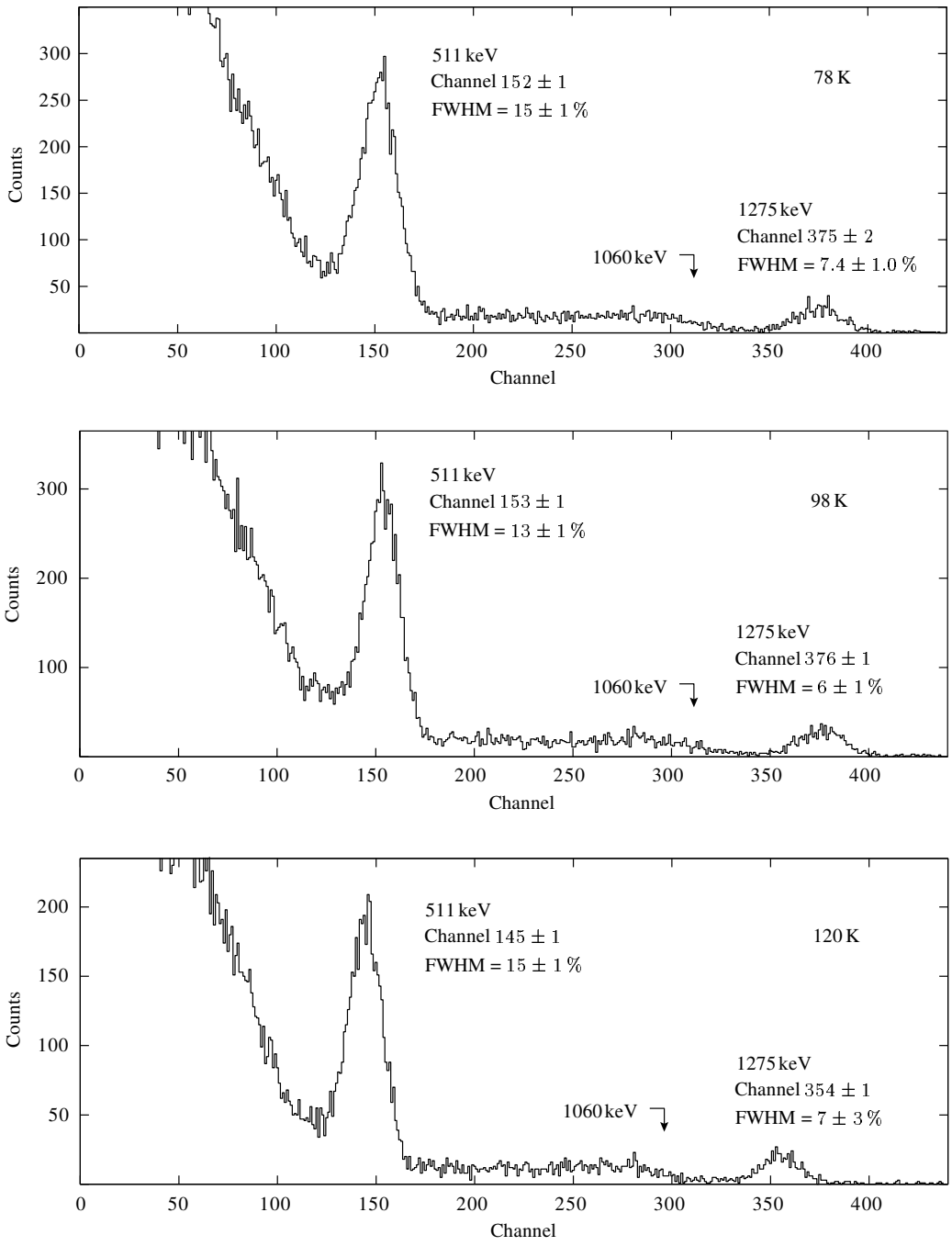

Figure 3.8: ^{22}Na pulse height spectra at three different temperatures including a fit of the peaks. A new photodiode was used for readout. The CsI crystal was painted with the Model Master dye.

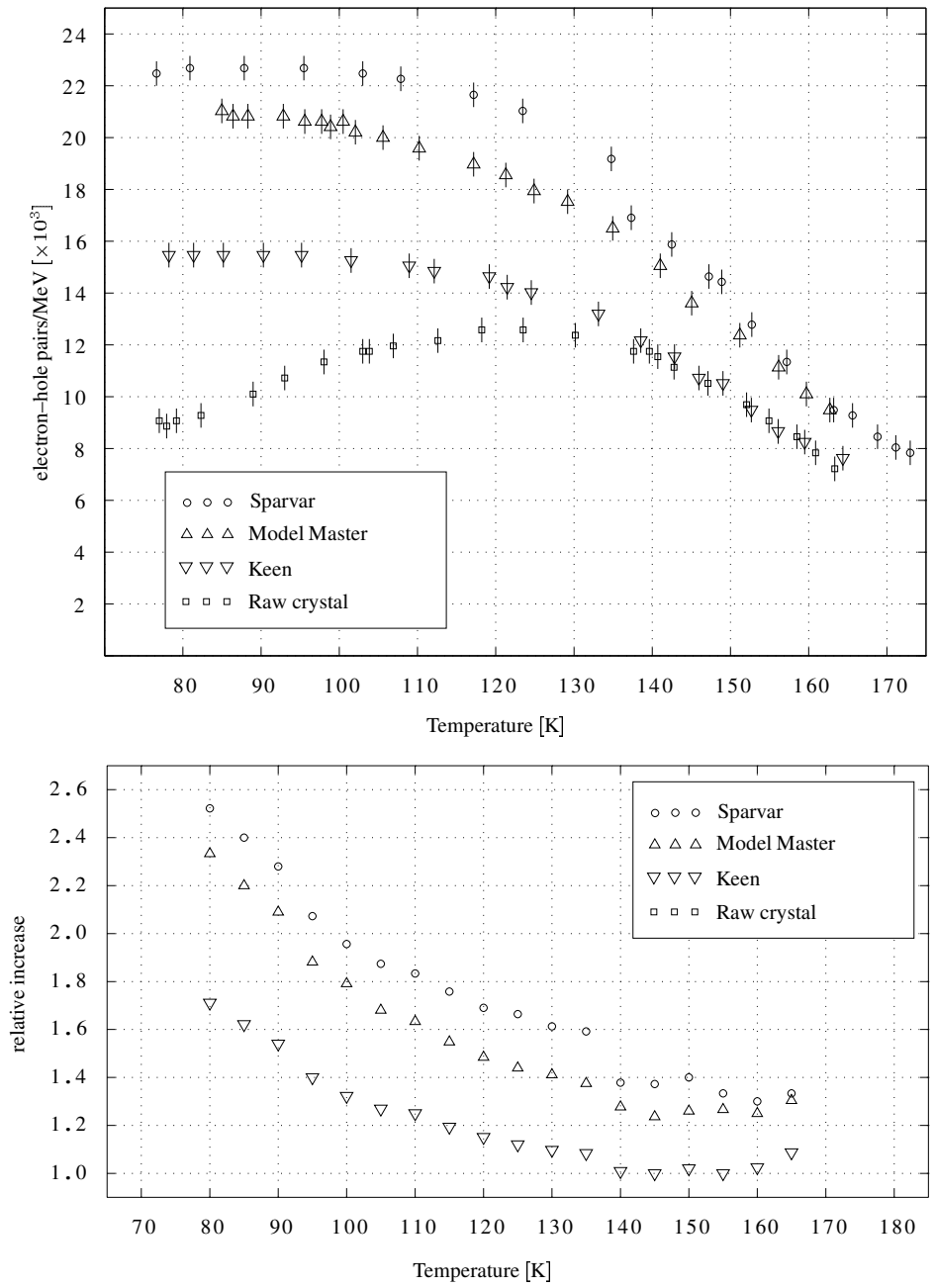

Figure 3.9: Upper Plot: Number of electron–hole pairs/MeV as a function of temperature. Pure CsI crystals were painted with wavelength shifting fluorescent dyes. For comparison, a measurement with a raw crystal is included. Lower Plot: Relative increase of the light yield of pure CsI by using wavelength shifting fluorescent dyes as compared to the raw crystal.

3.2.4 Comparison between Different Diodes

Photodiodes are very fragile devices and even little variations in the process of production (thickness and purity of the waver, doping concentrations) can change their quality significantly and can have great effect on their performance. Moreover, by mechanical, thermal or electrical stress a diode can be damaged easily. Therefore, even diodes which come from the same production cycle can vary greatly in their performance.

To find out if higher numbers than $12\,500 \pm 600$ electron–hole pairs (raw crystal) and $21\,000 \pm 600$ electron–hole pairs (crystal covered with Model Master dye) can be achieved, further measurements were taken out with three different SINTEF diodes. These diodes (diodes II – IV) were of the same type as the one used before (diode I). Two tests were made with every diode. One time with a pure CsI crystal without a wavelength shifter and one time with the Model Master dye. It turned out that a number of $28\,000 \pm 600$ electron–hole pairs/MeV can be reached with diodes II–IV in combination with the wavelength shifting dye (see figures 3.8 and 3.10). Compared to that figure, the produced number of

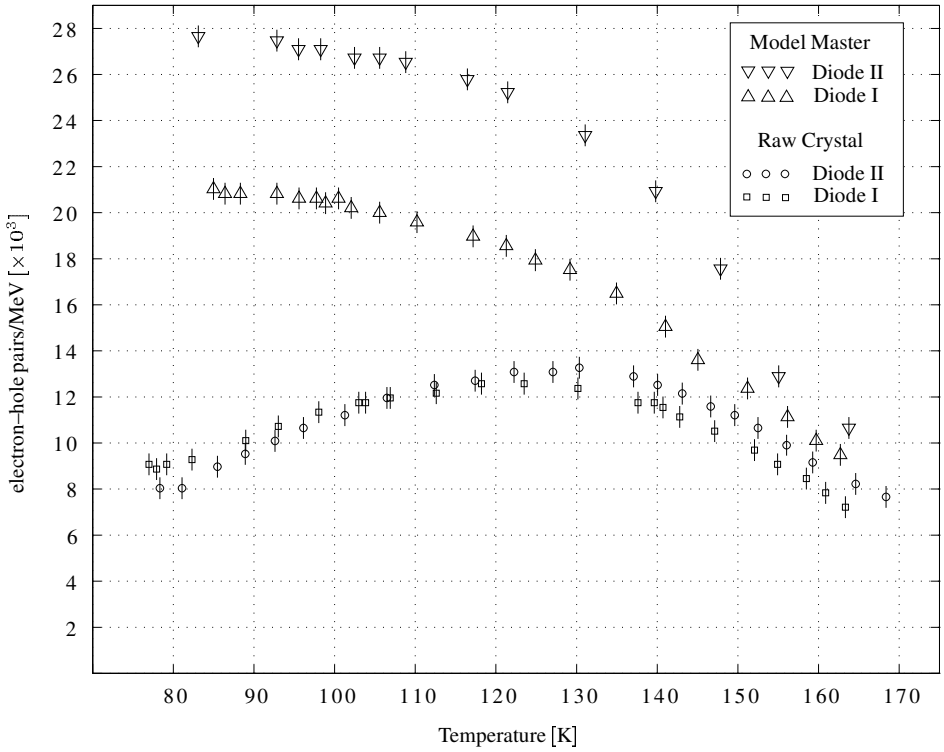

Figure 3.10: Comparison of two diodes in the number of electron–hole pairs/MeV as a function of temperature. One time the crystal was painted with the Model Master dye, the other time the crystal was unpainted.

$21\,000 \pm 600$ electron–hole pairs/MeV as shown in figure 3.9 is very low and can not be explained by normal fluctuations (all measurements were reproduceable, having fluctuations of $5-10\,\%$). These figures could lead to the conclusion that diode I has only three working pads. However, the two diodes show almost the same temperature dependence when the crystal is used without a wavelength shifter (see 3.10). This means that the the two diodes have a very different wavelength dependency. Diode I must have a much smaller quantum efficiency in the red part of the spectrum where the fluorescent dye emits light.

With other diodes up to 40 000 electron–hole pairs/MeV have been measured [5].

3.2.5 Light Yield Measurement with a Photomultilpier

To ensure that the measured dependence of light yield as a function of temperature is a unique characteristic of pure CsI, a different type of measurement has to be done for comparison.

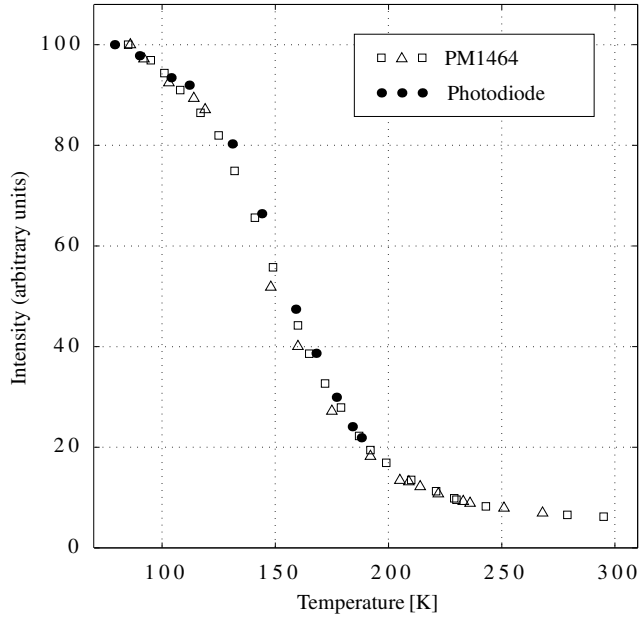

Figure 3.11: Relative intensity of the light yield of pure CsI as a function of temperature. Shown is a comparison between a measurement taken with a photomultiplier (Hamamatsu R1464) used for readout and another measurement taken with a photodiode (SINTEF). Only for the measurement with the photodiode the CsI crystal was painted with the Model Master dye.

A measurement of the total light yield of pure CsI as a function of temperature has been done previously with a Hamamatsu R1464 photomultiplier [2, 5]. To compare the two measurements both data sets were normalized to their maxima (see figure 3.11). The measurements are in good agreement. Thus, the observed light yield as a function of temperature seems to be a property of pure CsI only. However, the photomultiplier was held at room temperature during the measurement, whereas the photodiode was cooled down together with the crystal.

Possibly the quantum efficiency of the photodiode changes with temperature. For a direct comparison the photodiode either has to be kept at room temperature or its quantum efficiency as a function of temperature has to be measured.

3.2.6 Coupling of the Photodiodes to the CsI Crystal without Grease

In all previous measurements silicon grease was used to couple the photodiode to the crystal. To determine the influence of this procedure on the number of electron–hole pairs/MeV produced in the photodiode further tests were performed.

For this, the photodiode was layed directly on the polished surface of a CsI crystal. A crystal covered with the Model Master wavelength shifting dye was used for all measurements where no grease was used to couple the diode to the crystal.

The plot in figure 3.12 shows that the maximum number of electron–hole pairs/MeV at 77 K is only $16\,000 \pm 600$ compared to $21\,000 \pm 600$ if grease is used. This corresponds to an increase of 33 ± 6 %.

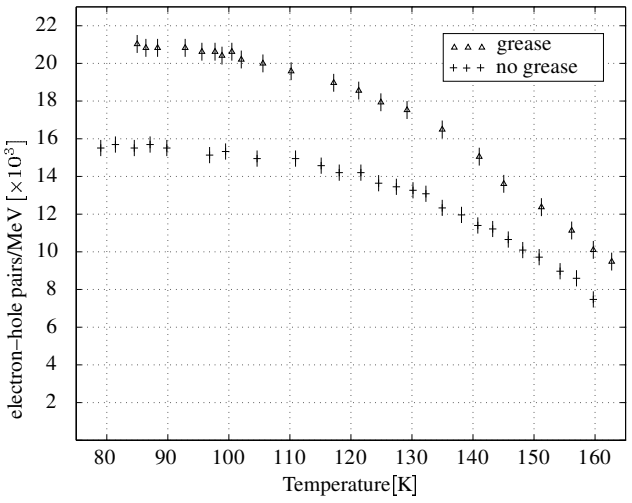

Figure 3.12: Number of electron–hole pairs/MeV as a function of temperature. The lower plot shows a measurement where no grease was used to couple the diode to the crystal. For comparison, a measurement where grease was used for coupling is included. Both times the crystal was painted with the Model Master dye.

In the plot of figure 3.13 all data was normalized to the maximum value of the measurements where no grease was used. Then the data without grease was scaled by factor 1.33. The shape of the curve as a function of temperature stays the same. The rise in efficiency is probably due to the reduced reflection on the surfaces of the diode and the crystal.

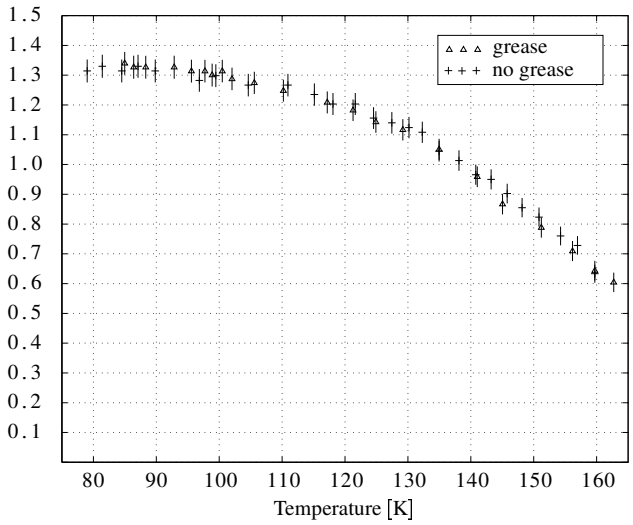

Figure 3.13: The relative efficiency as a function of temperature. To compare the two coupling methods (with or without grease), all data points (from figure 3.12) were normalized to the maximum value of the number of electron–hole pairs/MeV achieved using no grease. The latter were then scaled by factor 1.33.

3.3 Parameter Fit for Peak Evaluation

All ^{22}Na and ^{109}Cd pulse height spectra were fitted using the method of least squares. This method is suitable, if the errors are gaussian distributed. To obtain the best guess for the parameter vector $\vec{a}$, χ^2 has to be minimized:

$$\chi^2(\vec{a}) = \sum_{i=1}^{n} \frac{[y_i - f(x_i;\vec{a})]^2}{\sigma_i^2} \tag{3.11}$$

where $f(x_i;\vec{a})$ is the fit function, x_i the channel number, y_i the number of counts in channel x_i, $\vec{a}$ the parameter vector and $\sigma_i = \sqrt{y_i}$ the error of y_i.

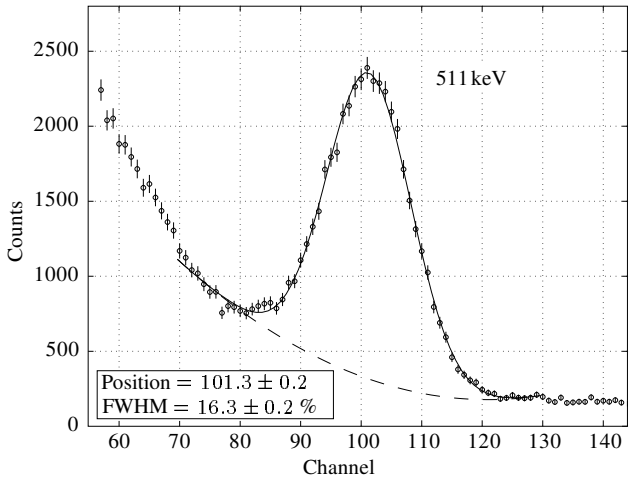

Figure 3.14: χ^2 fit of the 511 keV line of a measured ^{22}Na pulse height spectrum between channel 70 and 130, assuming a gaussian peak (solid line) and a quadratic background (dashed line).

The assumption, that the peaks are gaussian distributed and the background is quadratic seems to be reasonable (see figures 3.3, 3.6, 3.5, 3.8 and 3.14). The fit

function then reads:

$$f = \underbrace{a_1 + a_2 \cdot x + a_3 \cdot x^2}_{\text{quadratic background}} + \underbrace{\frac{a_4}{\sqrt{2\pi} \cdot a_6} \cdot \exp\left[-0.5\left(\frac{x - a_5}{a_6}\right)^2\right]}_{\text{gaussian distribution}} \tag{3.12}$$

with a_i, i=1,2,3 are the parameters of the quadratic background, a_4 is the area under the peak, a_5 the peak position and a_6 the standard deviation (FWHM/2.35). Since (3.12) is not linear in all parameters a_i, the algorithm of Marquardt, an iteration procedure, is used. This is a numerical iteration procedure which uses a linear Taylor expansion of $\chi^2(\vec{a})$. Details of this method can be found in [10].

Chapter 4

Test of the ATHENA Annihilation Detector

Before the completely assembled detector was inserted into the ATHENA experiment, a test at low temperature and an energy calibration had to be done. For this I designed a setup which is presented here together with first results of the performance of the 192 scintillating pure CsI crystals.

4.1 The Setup

The main components of the test setup were two steel pipes. The one with the larger diameter (pipe # 1) housed the detector, the lines for power supply and signal readout. The pipe with the smaller diameter (pipe # 2) was closed at the bottom and had an open end at the top. When it was inserted into pipe # 1, the volume in which the detector was placed was vacuum tight and radioactive sources could be lowered from outside close to the detector (see figure 4.1). A pressure of 10^{-6} mbar could be reached. To cool the detector down, the system was set into a dewar filled with liquid nitrogen.

A photograph of the setup including the vacuum pump and the vacuum gauge can be seen in figure 4.2.

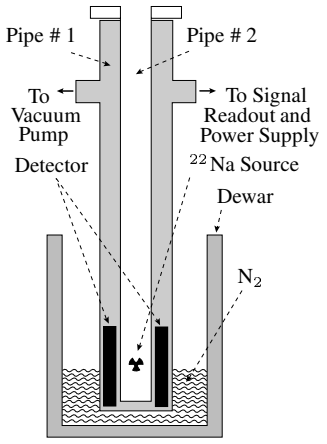

Figure 4.1: Test setup for the completely assembled ATHENA detector.

Figure 4.2: Photograph of the test setup with the vacuum pump and vacuum gauge. On the left hand side signal readout and power supply was connected.

4.2 Performance of the Detector

To test the performance of the scintillating CsI crystals of the detector a ^{22}Na source was lowered into pipe # 2 (see figure 4.1). The thickness d of the pipe was about 1 mm. With the density $\rho \simeq 7.9\,\mathrm{g\,cm^{-3}}$ of Fe and the absorption length $\lambda \simeq 10\,\mathrm{g\,cm^{-2}}$ for 511 keV γ's passing through Fe the γ intensity I was still sufficient:

$$I = I_0 \cdot \exp\left[-\frac{d \cdot \rho}{\lambda}\right] \simeq 92\,\% \tag{4.1}$$

The plot in figure 4.3 shows the positions of the 511 keV peaks of each crystal and the signal/noise ratio. The mean of the signal/noise ratio was 15.5 which is sufficient to detect 511 keV γ's from $e^+ - e^-$ annihilation. The measurements were done at a temperature of 137 K. A table of the 511 keV peak positions for all 192 CsI crystals can be found in appendix A.

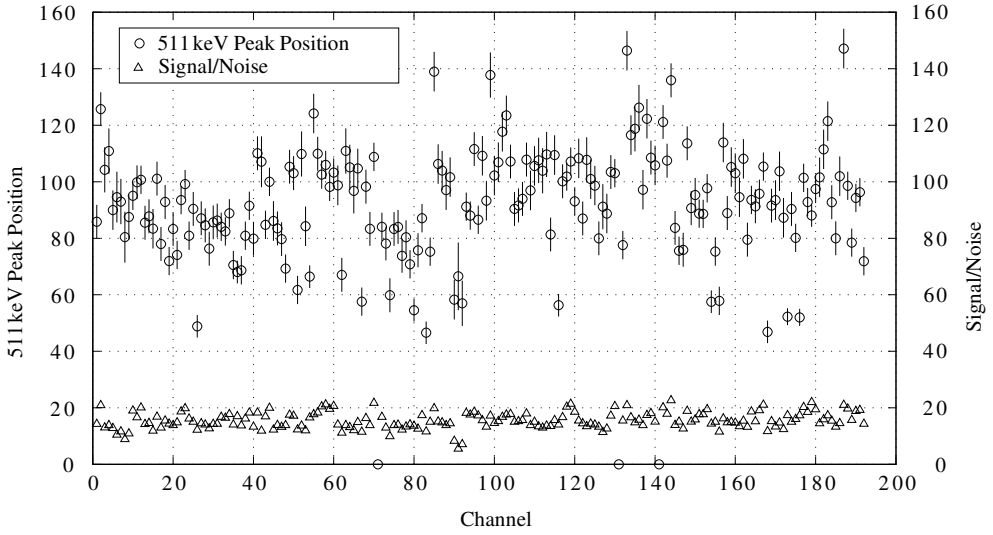

Figure 4.3: 511 keV peak position and signal/noise for each of the 192 pure CsI crystals of the ATHENA annihilation detector taken with a ^{22}Na source at 137 K.

A histogram of the 511 keV peak position is shown in figure 4.4. It was fitted with a Gaussian distribution:

$$y = y_0 + A \cdot \exp\left[\frac{(x - x_0)^2}{z}\right] \tag{4.2}$$

with $y_0 =$ offset, $A =$ height, $x_0 =$ center and $z =$ width of the distribution.

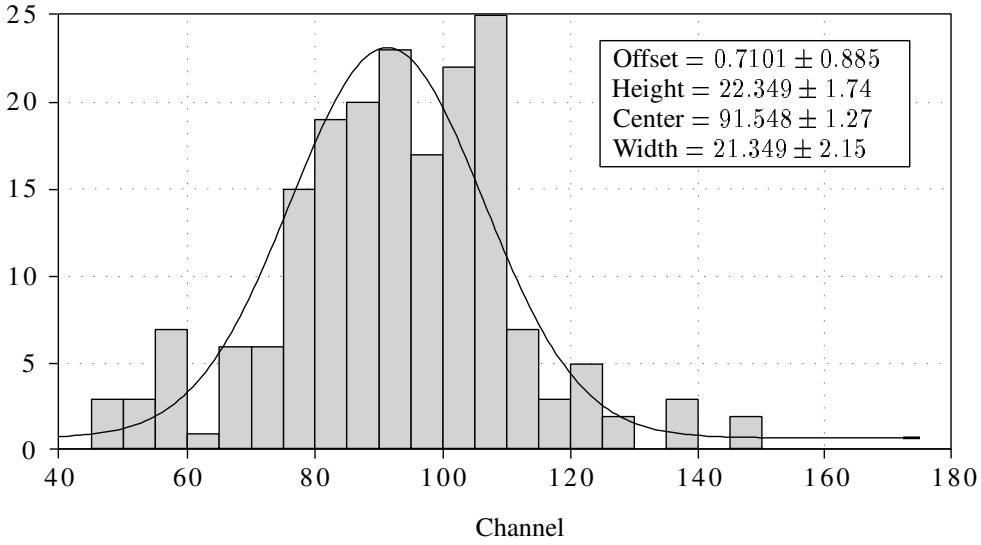

Figure 4.4: Histogram of the 511 keV peak position.

Pulse height spectra of the first row of 12 crystals can be seen in figure 4.5. The number of counts rises from crystal 1 to 5 and then decreases from crystal 6 to 12. Since all crystals were exposed to the γ radiation for the same time and the 16 rows were positioned vertically this means that the source was located around crystal 3-4.

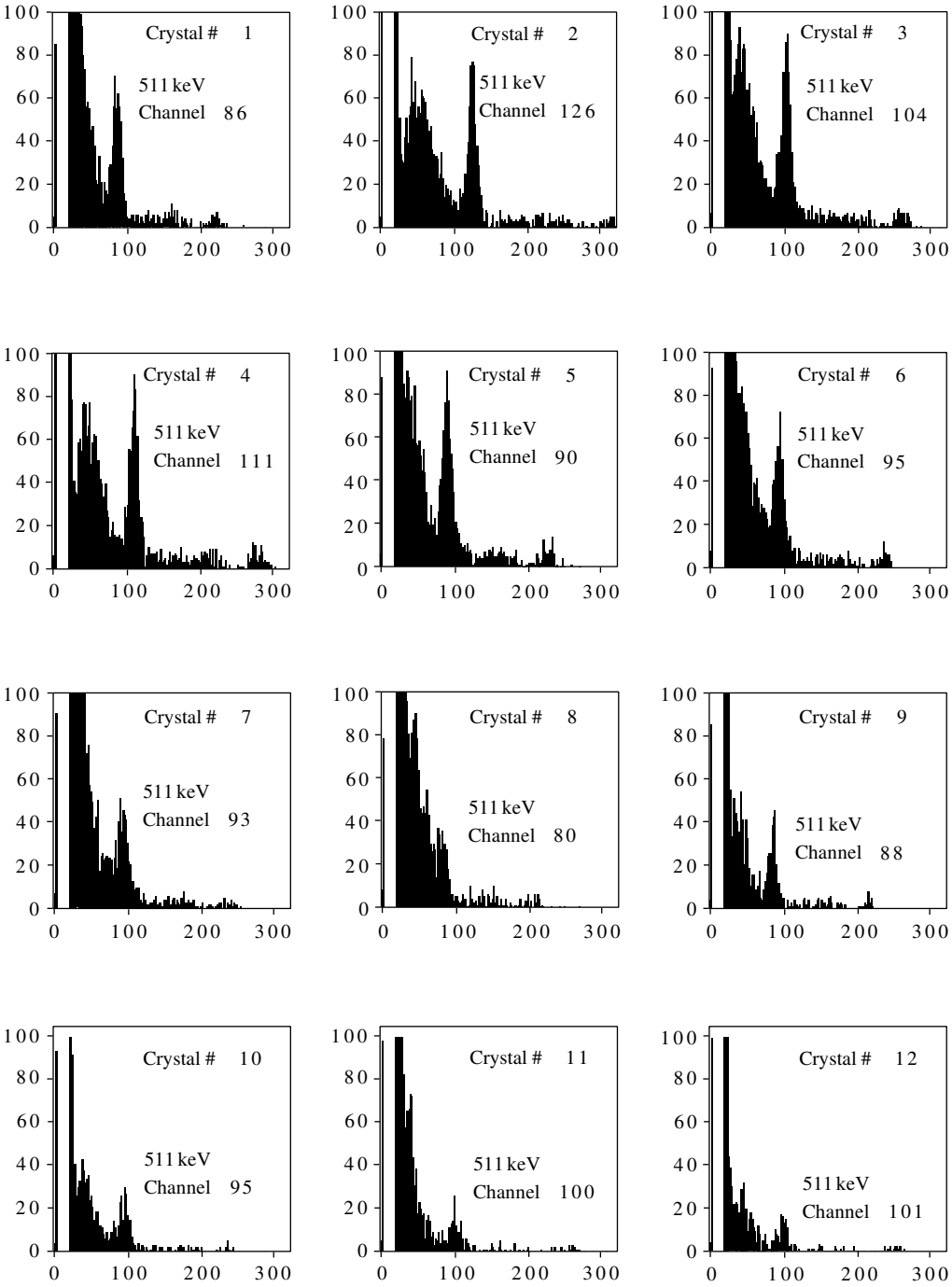

Figure 4.5: ^{22}Na pulse height spectra from one row of the annihilation detector taken at 137 K.

Chapter 5

Conclusions

With photodiodes used for readout of scintillation light it could be shown that the light yield of pure CsI increases with increasing temperature in the range between 77 K and 120 K where it reaches a maximum before falling again with increasing temperature in the range between 120 K and 165 K. $9\,000 \pm 600$ electron–hole pairs/MeV could be measured at 77 K, $12\,500 \pm 600$ at 120 K and $7\,000 \pm 600$ at 165 K. In contrast, it was observed earlier with photomultipliers that the light yield of pure CsI increases with decreasing temperature [5, 2]. The light yield of pure CsI as a function of temperature as measured with a photodiode in the range between 120 K and 165 K can be explained by the shift of the maximum of the emission spectrum of pure CsI to longer wavelengths at low temperature since the quantum efficiency of the SINTEF photodiodes is higher at longer wavelengths. In order to fully understand the drop in efficiency below 120 K additional measurements of the emission spectrum of pure CsI as a function of temperature have to be done and the quantum efficiency of the SINTEF photodiodes as a function of temperature has to be measured.

To better match the quantum efficiency of the photodiodes with the spectrum of scintillation light the use of wavelength shifters was investigated. It could be shown that fluorescent dyes are highly suitable for this purpose. Qualitatively all dyes had the same influence on the efficiency of scintillating pure CsI with photodiode readout. Not only did they improve the total efficiency up to a factor of 2.5, they also modified significantly the temperature characteristics. The maximum at 120 K disappeared. Instead, the highest efficiency was observed at 77 K and stayed constant with increasing temperature up to 100 K. From that point on efficiency decreased with increasing temperature. In conjunction with the Model Master wavelength shifting dye and photodiode readout a maximum of $27\,800 \pm 600$ electron–hole pairs/MeV could be measured in the range between 77 K and 100 K. At 120 K the efficiency had dropped to $89 \pm 4\,\%$ of the maximum then it deacreased linearly with increasing temperature down to $41 \pm 5\,\%$ at 165 K.

Using silicon grease to couple the photodiode to the crystal increases the number of electron–hole pairs by $33 \pm 6\,\%$. The grease obviously has a refractive index which prevents the scintillation light from being reflected at the crystal surface and at the diode surface respectively.

Large fluctuations in the performance of different diodes were observed. The diodes and crystals withstand many cooling cycles without changing their behavior.

First tests of the completely assembled detector at low temperature were successful. For 511 keV γ's an average signal/noise ratio of 15.5 could be reached, which is sufficient to detect $e^+ - e^-$ annihilations.

The most important implications for the ATHENA annihilation detector are:

- Fluorescent dyes should be used to enhance the scintillation light yield of pure CsI as seen by photodiodes.
- The Model Master dye is the most promising one. It withstood more cooling cycles than all other dyes and led only to a 10 % lower number of electron–hole pairs/MeV compared to the best dye (Sparvar).
- When wavelength shifters are used, the operating temperature is not critical in the range between 77 K and 130 K since changes in light yield are relatively low (at 130 K the measured light yield is still 85 % of the maximum value at 77 K).
- Silicon grease should be used to couple the diodes to the crystals.
- The characteristics of both diodes and crystals stay constant for many cooling cycles.

Appendix A

Detector Performance

Positions of the 511 keV peaks listed for all 192 CsI crystals of the ATHENA annihilation detector as achieved in a first test at 137 K using a ^{22}Na source.

Row I

Crystal #	511 keV Peak	Error
1	86	6
2	126	6
3	104	8
4	111	-
5	90	7
6	95	9
7	93	8
8	80	9
9	88	-
10	95	5
11	100	6
12	101	5

Row II

Crystal #	511 keV Peak	Error
13	85	6
14	88	6
15	83	7
16	101	6
17	78	6
18	93	6
19	72	5
20	83	6
21	74	5
22	94	5
23	99	5
24	81	5

Row III

Crystal #	511 keV Peak	Error
25	90	6
26	49	4
27	87	6
28	85	6
29	76	6
30	86	6
31	86	6
32	84	5
33	82	5
34	89	-
35	70	5
36	68	4

Row IV

Crystal #	511 keV Peak	Error
37	69	5
38	81	5
39	92	5
40	80	6
41	110	6
42	107	9
43	85	5
44	100	5
45	86	7
46	83	6
47	80	6
48	69	5

Row V

Crystal #	511 keV Peak	Error
49	105	6
50	103	6
51	62	5
52	110	8
53	84	-
54	66	4
55	124	7
56	110	6
57	103	5
58	106	-
59	98	5
60	103	5

Row VI

Crystal #	511 keV Peak	Error
61	98	7
62	67	6
63	110	8
64	105	8
65	97	8
66	105	7
67	58	5
68	98	6
69	83	-
70	109	5
71	-	-
72	84	5

Row VII

Crystal #	511 keV Peak	Error
73	78	6
74	60	6
75	83	6
76	84	6
77	74	6
78	80	6
79	71	5
80	55	4
81	76	6
82	87	5
83	47	4
84	75	5

Row VIII

Crystal #	511 keV Peak	Error
85	139	7
86	106	6
87	104	6
88	97	7
89	102	7
90	58	-
91	67	12
92	57	8
93	91	5
94	88	5
95	112	6
96	87	5

Row IX

Crystal #	511 keV Peak	Error
97	109	7
98	93	7
99	138	8
100	102	7
101	107	7
102	118	7
103	123	7
104	107	6
105	90	6
106	92	6
107	94	6
108	108	6

Row X

Crystal #	511 keV Peak	Error
109	97	7
110	106	7
111	108	8
112	104	8
113	110	8
114	81	6
115	109	7
116	56	4
117	100	6
118	102	5
119	107	5
120	93	5

Row XI

Crystal #	511 keV Peak	Error
121	108	7
122	87	6
123	108	8
124	101	7
125	99	7
126	80	6
127	91	8
128	89	7
129	103	6
130	103	5
131	-	-
132	78	5

Row XII

Crystal #	511 keV Peak	Error
133	146	7
134	117	7
135	119	8
136	126	8
137	97	7
138	122	7
139	109	6
140	106	7
141	-	-
142	121	6
143	107	6
144	136	6

Row XIII

Crystal #	511 keV Peak	Error
145	84	6
146	76	5
147	76	6
148	114	6
149	91	6
150	95	6
151	89	5
152	89	5
153	98	5
154	58	4
155	75	5
156	58	5

Row XIV

Crystal #	511 keV Peak	Error
157	114	7
158	89	6
159	105	7
160	103	7
161	95	7
162	108	7
163	79	6
164	94	5
165	91	6
166	96	5
167	105	5
168	47	4

Row XV

Crystal #	511 keV Peak	Error
169	92	6
170	94	7
171	104	7
172	87	7
173	52	3
174	90	6
175	80	5
176	52	3
177	101	5
178	93	5
179	88	
180	97	5

Row XVI

Crystal #	511 keV Peak	Error
181	102	7
182	111	-
183	121	7
184	93	6
185	80	6
186	102	7
187	147	7
188	99	5
189	78	5
190	94	5
191	96	5
192	72	5

Bibliography

[1] C. Regenfus. *Antihydrogen production and precision experiments on trapped cold antihydrogen*. Hyperfine Interactions, 119:301–304, 1999.

[2] P. Niederberger. *Untersuchung von CsI–Szintillatoren bei tiefen Temperaturen*. Diplomarbeit, Physik–Institut der Universität Zürich, June 1999.

[3] Glenn F. Knoll. *Radiation Detection and Measurement*. John Wiley & Sons, Inc., third edition, 2000.

[4] C.L. Woody et al. *Readout Techniques and Radiation Damage of undoped Cesium Iodide*. IEEE Transactions on Nuclear Science, 37(2), April 1990.

[5] C. Amsler et al. *Temperature Deoendence of Pure CsI Scintillation Light Yield and Decay Time*. Nuclear Instruments and Methods, to be published, 2001.

[6] Gerhard Lutz. *Semiconductor Radiation Detectors*. Springer, 1999.

[7] K. Debertin and R.G. Helmer. *Gamma– and X–Ray Spectrometry with Semiconductor Detectors*. North–Holland, 1988.

[8] S.M. Sze. *Semiconductor Devices*. John Wiley & Sons, 1985.

[9] H. Nishimura, M. Sakata, T. Tsujimoto and M. Nakayama. *Origin of the 4.1 eV luminescence in pure CsI scintillator*. Physical Review B, 51(4), July 1994.

[10] Hendrik S. Pruys. *Skript zur Vorlesung Datenanalyse*. Physik–Institut der Universität Zürich, 1998.

Acknowledgements

A year and a half ago Hendrik Pruys asked me if I would be interested in writing my diploma thesis at CERN in the group of Claude Amsler. After a visit in Geneva a few weeks later, I knew that I would like to do so. Now that I finished my thesis, I know that I made a good choice. It was a very interesting time for me and I learned a lot about experimental physics (and a few words of french).

I thank Claude Amsler for giving me the opportunity to come to CERN and join the ATHENA group. His support regarding my thesis on pure CsI as well as regarding all organisational matters contributed greatly to my feeling that it was a worthwhile year for me.

Christian Regenfus willingly shared with me his knowledge of experimental physics in general and of the ATHENA annihilation detector in particular. Large parts of the investigations on pure CsI that are presented in this thesis I could not have done without his assistance.

Thanks to David Lindelöf for his help. The observations of the quantum efficiency of the SINTEF photodiodes and the first measurements with the completely assembled detector at low temperature were done by him. He also discovered the Model Master wavelength shifting dye.

A special thank to Hendrik Pruys for encouraging me to come to CERN and for his support throughout the year. Discussions with him were always pleasant and constructive.

For the future I wish the whole ATHENA collaboration lots of antihydrogen for interesting physics.